Journal of Psychiatric Research 166 (2023) 100–114

Contents lists available at ScienceDirect

Journal of Psychiatric Research

journal homepage: www.elsevier.com/locate/jpsychires

Impaired myelin ultrastructure is reversed by citalopram treatment in a mouse model for major depressive disorder

Ifat Israel-Elgali [a,b], Hope Pan [c], Keren Oved [b], Nir Pillar [b], Gilad Levy [a], Boaz Barak [a,d], Ana Carneiro [c], David Gurwitz [a,b,*], Noam Shomron [a,b,e,f,**]

[a] Sagol School of Neuroscience, Tel-Aviv University, Tel Aviv, Israel
[b] Faculty of Medicine, Tel Aviv University, Tel Aviv, Israel
[c] Department of Pharmacology, Center for Molecular Neuroscience, Vanderbilt University School of Medicine, Nashville, TN, USA
[d] Faculty of Social Sciences, School of Psychological Sciences, Tel Aviv University, Tel Aviv, Israel
[e] Edmond J Safra Center for Bioinformatics, Tel Aviv University, Tel Aviv, Israel
[f] Tel Aviv University Innovation Laboratories (TILabs), Tel Aviv, Israel

ARTICLE INFO

Keywords:
Major depression disorder
SSRI
Chronic unpredictable stress
microRNA
Myelin

ABSTRACT

Major depressive disorder (MDD) is the most common and widespread mental disorder. Selective serotonin reuptake inhibitors (SSRIs) are the first-line treatment for MDD. The relation between the inhibition of serotonin reuptake in the central nervous system and remission from MDD remains controversial, as reuptake inhibition occurs rapidly, but remission from MDD takes weeks to months. Myelination-related deficits and white matter abnormalities were shown to be involved in psychiatric disorders such as MDD. This may explain the delay in remission following SSRI administration. The raphe nuclei (RN), located in the brain stem, consist of clusters of serotonergic (5-HT) neurons that project to almost all regions of the brain. Thus, the RN are an intriguing area for research of the potential effect of SSRI on myelination, and their involvement in MDD. MicroRNAs (miRNAs) regulate many biological features that might be altered by antidepressants. Two cohorts of chronic unpredictable stress (CUS) mouse model for depression underwent behavioral tests for evaluating stress, anxiety, and depression levels. Following application of the CUS protocol and treatment with the SSRI, citalopram, 48 mice of the second cohort were tested via magnetic resonance imaging and diffusion tensor imaging for differences in brain white matter tracts. RN and superior colliculus were excised from both cohorts and measured for changes in miRNAs, mRNA, and protein levels of candidate genes. Using MRI-DTI scans we found lower fractional anisotropy and axial diffusivity in brains of stressed mice. Moreover, both miR-30b-5p and miR-101a-3p were found to be downregulated in the RN following CUS, and upregulated following CUS and citalopram treatment. The direct binding of these miRNAs to *Qki,* and the subsequent effects on mRNA and protein levels of myelin basic protein (*Mbp*), indicated involvement of these miRNAs in myelination ultrastructure processes in the RN, in response to CUS followed by SSRI treatment. We suggest that SSRIs are implicated in repairing myelin deficits resulting from chronic stress that leads to depression.

1. Introduction

Major depressive disorder (MDD) is a complex, common, and recurrent mental disorder (Sullivan et al., 2000) It is among the leading global causes of disability (Lopez et al., 2006), affecting more than 250 million people annually (Depressive disorder), and is more commonly diagnosed in women than in men (Hasin et al., 2018). The monoamine hypothesis of depression, formulated over 40 years ago, proposes the biological basis of depression results from a central nervous system (CNS) imbalance or decrease in the neurotransmitter serotonin (5-HT) (Mohammad-Zadeh et al., 2008). This decrease might be due to increased serotonin transporter (SERT) activity, reduced serotonin synthesis in the CNS or damage to CNS serotonergic synapses following chronic stress conditions (Hirschfeld, 2000; Czéh et al., 2016). Thus, the current first-line treatment for MDD is selective serotonin reuptake inhibitors (SSRIs), which are antidepressant drugs that block serotonin

* Corresponding author. Sagol School of Neuroscience, Tel-Aviv University, Tel Aviv, Israel.
** Corresponding author. Sagol School of Neuroscience, Tel-Aviv University, Tel Aviv, Israel.
E-mail addresses: gurwitz@tauex.tau.ac.il (D. Gurwitz), nshomron@tauex.tau.ac.il (N. Shomron).

https://doi.org/10.1016/j.jpsychires.2023.09.012
Received 29 May 2023; Received in revised form 24 July 2023; Accepted 15 September 2023
Available online 16 September 2023
0022-3956/© 2023 The Authors. Published by Elsevier Ltd. This is an open access article under the CC BY license (http://creativecommons.org/licenses/by/4.0/).

reuptake by binding to SERT (Sangkuhl et al., 2009).

The monoamine hypothesis suggests that SSRIs relieve depression symptoms mainly via blocking SERT, thereby increasing the availability of serotonin in serotonergic CNS synapses (Hirschfeld, 2000; van Praag et al., 1987; Price et al., 1990). However, while SERT inhibition is achieved within a few days of initiating SSRI treatment, remission from depression starts after about 4 weeks (Gelenberg, 2010; Rayner et al., 2011; Cipriani et al., 2012). This discrepancy in time led to the suggestion that recovery from depression involves synaptogenesis and neurogenesis (Eisch and Petrik, 2012; Bambico et al., 2013; Mateus-Pinheiro et al., 2013; Oved et al., 2013). However, it is unclear whether SSRI-mediated SERT blockage is involved in these two processes (Moncrieff et al., 2022).

The raphe nuclei (RN) are a cluster of nuclei found in the brain stem, consisting of serotonergic synthesizing neurons which assemble the major ascending serotonergic fibers projecting to the forebrain and descending fibers that extend to the medulla and spinal cord (Steinbusch and Nieuwenhuys, 1981; Commons, 2020). Through its ascending projections, the RN has an important role in the regulation of many physiological functions, including learning, cognition, and mood (Michelsen et al., 2008).

Myelin is a lipid-rich electrically insulating tissue crucial for electrical communication and transmission of axon potentials between neurons, and that provides metabolic support to the axons it ensheaths (Nave, 2010). Oligodendrocytes are the myelinating cells of the CNS. They are generated from oligodendrocyte progenitor cells and are essential for myelin formation and regeneration, for example, in multiple sclerosis (Bradl and Lassmann, 2010; Franklin and Ffrench-Constant, 2017). A main protein in myelin is myelin basic protein (MBP), expressed on the cytoplasmic surface of the oligodendrocyte plasma membrane (Kuhn et al., 2019). Oligodendrocytes express serotonin receptors and were shown to be affected by serotonin, 5-HT receptor agonists and SSRI administration (Fan et al., 2015; Kurokawa et al., 2021).

Myelination related deficits, oligodendrocyte morphometry changes, and white matter abnormalities were previously shown to be involved in various psychiatric disorders such as schizophrenia, alcoholism, bipolar disorder and MDD (Hakak et al., 2001; Tkachev et al., 2003; Hamidi et al., 2004; Rajkowska et al., 2015, 2018; Miguel-Hidalgo et al., 2017, 2019; Miguel-Hidalgo, 2023). Most importantly, the prevalence of MDD and anxiety disorders among individuals with multiple sclerosis, a demyelinating disease of the CNS, highlights the connection between myelin deficits and MDD symptoms (Joffe et al., 1987; Chwastiak and Ehde, 2007). Certain studies showed no change in oligodendrocyte density in MDD, suggesting unchanged morphology despite possible organizational disruption (Williams et al., 2015; Öngür et al., 1998). The disruption might result from altered myelin-related gene expression or splicing (Aston et al., 2005; Klempan et al., 2009a; Darbelli et al., 2017); and consequently present in myelin related proteins, or as abnormalities in transcription factors of myelin-related genes (Tham et al., 2011).

MicroRNAs are single-stranded, short endogenous non-coding RNAs present in all cells and tissues that down-regulate gene expression at the post-transcriptional level (Rukov and Shomron, 2011). Thousands of miRNAs are encoded within the human or rodent genome (Londin et al., 2015), and their dysregulation has been implicated in many chronic diseases, including brain disorders (Modai and Shomron, 2016; Serafini et al., 2014a). As changes in miRNA levels affect global gene expression (Lim et al., 2005), miRNAs have been proposed as biomarkers for disease diagnosis and treatment choice (Rukov et al., 2011, 2014), including for CNS disorders (Gurwitz, 2019). MiRNAs have been related to neuro-inflammation, altered neurogenesis, neuroplasticity, stress response and circadian rhythms, and factors implicated in MDD pathogenesis (Dwivedi, 2013; Forero et al., 2010; Fiore et al., 2008; Im and Kenny, 2012); all of which may be affected by antidepressant treatment (D'Sa and Duman, 2002).

Here, we aimed to explore the interrelationships between the effects of the SSRI citalopram on relief from depression-like symptoms, RN myelin integrity, and RN microRNA expression in the chronic unpredictable stress (CUS) mouse model for depression. Our findings showed that chronic stress caused depressive-like symptoms and RN defects in myelin structure, which were prevented by daily citalopram administration and were correlated with the expression levels of miR-30b-5p and miR-101-3p, two miRNAs which target the gene *Qki*. Accordingly, elevated *Qki* expression levels were observed in the RN of CUS mice, which affected *Mbp* expression and myelin structure – all of which prevented by citalopram. Our study suggests that the capacity of citalopram to restore normal myelin structure may be implicated in its mode of antidepressant action.

2. Materials & methods

2.1. Animals, treatment and CUS

A total of 23 male C57BL/6, 6 weeks old mice were tested in the first cohort experiment, and 48 male C57BL/6, 6 weeks old mice were tested in the second cohort. Male mice were used in order to avoid effects of female hormonal cycles on the results. The experiment was designed where in the 1st cohort, 6 mice were subjected to Chronic Unpredictable Stress (CUS) and given water, 6 mice exposed to CUS and given citalopram hydrobromide (10 mg/kg/day) in drinking water (0.1 mg/ml), 6 mice were given citalopram in drinking water and 5 mice were used as controls and given water. In the second cohort, 12 CUS-exposed mice were given vehicle via *i.p.* injection, 12 mice exposed to CUS were given citalopram hydrobromide (10 mg/kg/day) (C7861, Sigma-Aldrich, USA) via *i.p.* injection, 12 mice were given citalopram via *i.p.* injection and 12 mice were used as controls and given vehicle via *i.p.* injection.

CUS protocols entailed a randomized six-week schedule of daily mild stressors, which started when mice were 6 weeks old. Treatment (vehicle or citalopram) was given at the start of the fourth week (*i.e.* mice were 9 weeks old), for three weeks. Additionally, mice were weighed on the first day of each of the six weeks of CUS and nestlet measurements were made on the days following a "change to new cage" stressor.

Every mouse in a given cohort in the CUS groups, was exposed to the same stressor on a given day. Stressful stimuli were administered at a random time of day, though always during the light portion of the controlled light/dark cycle. Following six weeks of CUS exposure, behavioral tests were performed to quantify the effects of this stress.

Each stressed mouse was housed individually, while control mice were group housed (maximum of 5 mice) and remained in their home cages throughout, in the Vanderbilt Murine Neurobehavioral Core during the first cohort, or in the conventional murine center at the Faculty of medicine at Tel Aviv University during the second cohort, with controlled 12-h light/dark cycles, freely available food and water, and controlled temperature and humidity. All experimental procedures were approved by the Vanderbilt Institutional Animal Care and Use Committee under the protocol M/15/014, or by the Tel Aviv University Institutional Animal Care and Use Committee under the protocol TAU-MD-IL-2206-167-5.

2.2. Stressors

Each day was randomly assigned one of six possible stressors or as a rest day (no stressor).

1 Changing to a New Cage. This stressor consisted of removing a mouse from its home cage and rehousing it in a new, clean cage. No bedding, food or water was carried over to the new housing. A nestlet was placed in the new cage.
2 Confinement to Plastic Cylinder. This stressor consisted of removing the mouse from its home cage and placing it in a restraint tube for 5 min. After the period of confinement, the mouse was returned to its unaltered home cage.

3 Shaking of Home Cage. This stressor consisted of shaking the mouse home cage three times by hand for a duration of 30 s each, with a 1-min interval between each shaking. The home cage is shaken with enough force so that the mouse displays tonic immobility.
4 Exposure to Water. Each mouse was removed from its home cage and placed in a 500 ml beaker containing 1 cm of water at room temperature for 6 min. Mice were hand-dried and returned to their home cage.
5 Swapping Home Cage of Two Mice. This stressor consisted of removing two mice from their respective home cages and rehousing them in each other's home cages. No bedding, food or water were replaced or swapped between cages. Mice remained in their new home cage until the next cage swap stimulus, or until the conclusion of the six weeks of CUS.
6 Tilt cage. In this stressor mice remained in their respective cages while cages were tilted to 45° for a duration of 2 h.
7 Rest day. No stress stimulus was administered. Mice remained in their unaltered home cages.

2.3. Behavioral testing

Animals were tested during the light phase, and acclimated to testing room conditions for 30 min. All apparatuses were cleaned with chlorine dioxide disinfectant (Vimoba, Quip Labs, Wilmington, DE) prior to the first testing session and between sessions. Mice were tested in a randomized order for each test. Test order was designed to minimize carryover anxiety on subsequent assays. Individual tests were conducted with a minimum of 24 h between each test.

2.3.1. Forced swim test (FST)

The forced swim test is used to evaluate depressive like behavior. The apparatus is a clear Plexiglas cylinder, 24 cm high and 19 cm in diameter, filled with approximately 16 cm of water at 23 °C. In the test, the mouse was placed in the cylinder for 7 min and then moved to a heated cage until the fur dried completely. Typically, the mouse gradually stopped swimming before being removed. Water was changed and the apparatus cleaned between each test. Immobility duration, the time the mouse remained floating motionless was measured during the last 5 min. All tests were filmed by video camera. A blind competent observer scored immobility for the first cohort, while the second cohort was tracked and analyzed using EthoVision XT (Noldus IT, Netherlands). Latency to first immobile period and total immobility were recorded.

2.3.2. Elevated plus maze (EPM)

The elevated plus maze is used to evaluate anxiety like behavior. The apparatus consists of a four-armed platform (+shape) elevated 40 cm off the ground. Two arms are "closed" and confined by walls (15 cm high) and two arms are "open" with no walls. Each arm is 35 cm long and 5 cm wide, and similar arms face one another. In the test, each mouse is placed at the center of the EPM facing toward one of the closed arms and then allowed to move freely for 7 min. When the mice are placed on the maze, the video-tracking system, EthoVision XT (Noldus IT, Netherlands), starts. The respective number of entries into the open and closed arms and the time spent exploring each arm are recorded for each mouse. After 7 min of testing, mice were removed from the plus maze and placed back in their home cage outside the testing environment. The EPM was cleaned with Virusolve+ (Amity International, USA) before the next test.

2.4. Magnetic resonance imaging (MRI) and diffusion tensor imaging (DTI)

Forty-eight twelve-weeks old mice underwent MRI-DTI scans. During MRI sessions, anesthesia was induced and maintained using isoflurane (1.5%) in pure oxygen. A heating system was used to maintain the animal body temperature and their respiration was monitored and maintained at 30–50 breaths/min using a pneumatic balloon positioned against the animal's chest.

MRI was performed in the Strauss computational neuroimaging center at Tel Aviv University, by a Bruker Biospec 7T/30 Scanner equipped with a 660 mT/m gradient unit, using a cross coil configuration of 86 mm transmissive Volume coil and mouse quadrature coil as a receiver. The MRI scan protocol included structural T2 weighted (T2w) images that were acquired with the rapid acquisition with relaxation enhancement sequence (RARE) and Diffusion Tensor Imaging (DTI) acquisition with a Diffusion-Weighted Spin-Echo Echo-Planar-Imaging pulse sequence (DW-SE-EPI). T2w acquisition was done with the following parameters: TR = 2500 ms; effective TE: 30 ms, RARE factor 8 with 8 repetitions. 20 coronal slices, 0.6 mm thick (no gaps), with in-plane resolution of 0.1 mm2 covering the entire brain, and lasts 4:00 min. For DTI we have used TR/TE = 3000/22.3 ms, $\Delta/\delta = 10/2.5$ ms, 2 EPI segment, 30 gradient directions with b-value at 1000 s/mm2 and three B0 images. 28 axial slices, 0.6 mm thick (no gaps), with in-plane resolution of 0.175 mm2. The DTI acquisition took 10:00 min.

DTI dataset was corrected for head movement and eddy current distortion using ExploreDTI (Leemans et al., 2009) platform within MATLAB (2022a, The MathWorks, Inc., USA). Following the corrections, the dataset underwent non-linear tensor estimation with structural corrections to the anatomical T2w image. Several indices were extracted from DTI analysis, such as fractional anisotropy (FA), mean diffusivity (MD), and axial and radial diffusivities (AD and RD, respectively) that were then co-registered and normalized to a template mouse brain using SPM 12 (Statistical Parametric Mapping, London, UK). We performed an ANOVA test based on DTI indices between four groups of mice, where differences lower than alpha of 0.05 were considered significant. The p values were than plotted upon the template brain.

2.5. Tissue collection

For RNA extraction and western blotting experiments, mice were euthanized by rapid decapitation without anesthesia. For TEM experiments, mice were perfused according to TEM protocol (see section 14). Brains were harvested and midbrains were dissected by coronal sectioning of the brain at Bregma −4.24 mm and −5.02 mm. Superior colliculus and raphe-enriched sections were separated by making an incision at the aqueduct (Interaural 3.44 mm), where the tissue below the aqueduct was considered enriched in serotonergic cell bodies. Samples aimed for RNA extraction and western blotting experiments were snap frozen in liquid nitrogen, while samples for TEM or immunofluorescence experiments were kept in 4 °C according to TEM protocol.

2.6. RNA extraction

Twenty-three samples from the 1st cohort underwent RNA purification using phenol-chloroform extraction: Tissue samples were first homogenized with stainless steel beads and then lysed using TRIzol reagent (Thermo Fisher Scientific, USA), followed by RNA separation using chloroform and isopropanol precipitation. The final RNA concentrations and purity were measured using a NanoDrop ND-1000 spectrophotometer (NanoDrop Technologies, Thermo Fisher Scientific, USA).

2.7. miRNA profiling

The multiplexed NanoString nCounter miRNA expression assay (NanoString Technologies, Seattle, WA, USA) was used to profile ~800 mice miRNAs (according to the miRNAs included in the NanoString array) in the RN and SC derived RNA samples. The assay was performed according to the manufacturer's protocol (NanoString Technologies, 2020), and as was previously carried out in Shomron lab (Pillar et al., 2017). Analysis included adjustment of p-values for genome-wide

miRNA profiling, in order to prevent inflation of the false positive rate in multiple testing.

2.8. Reverse transcription (RT)-PCR

Reverse transcription reactions for mRNA and for specific mature miRNAs were performed using the High-Capacity cDNA Reverse-Transcription Kit with random primers or TaqMan miRNA assays, respectively, according to the manufacturer's recommendations (Thermo Fisher Scientific, USA).

2.9. Polymerase chain reaction (PCR)

Amplification of specific mRNA regions was performed using cDNA, by Polymerase Chain Reaction (PCR), using KAPA2G Fast HotStart ReadyMix (KK5609, Sigma-Aldrich, USA) and custom planned primers (Supplementary Table 1). PCR products were loaded and run through a 1.5% agarose gel. Bands signal was detected via FluorChem M camera (Bio-techne, Minneapolis, USA) and analyzed using ImageJ software (National Institutes of Health; NIH).

2.10. Real-time quantitative PCR

Real-time polymerase chain reaction (PCR) was performed to validate top significant candidates obtained by mRNA sequencing and the NanoString nCounter miRNA assay, according to the manufacturer's protocol (Thermo Fisher Scientific, USA). MiRNA and mRNA expression was tested using TaqMan universal PCR Master Mix (Thermo Fisher Scientific, USA) and Quanta qPCR Gene Expression Master Mix (Quanta Technology, USA), respectively. PCR amplification and analysis were performed using the StepOne Real-Time PCR System (Thermo Fisher Scientific, USA). Comparative critical threshold (Ct) values, obtained by real-time PCR analysis, were used for relative quantification of gene or miRNA expression, and determination of the fold-change of expression. Fold change values were obtained by using the formula: $2-\Delta\Delta Ct$ (Schmittgen and Livak, 2008). Normalization for miRNA and mRNAs was performed compared to mouse SnoRNA202 and mouse *Gapdh* expression, respectively, control genes which exhibited stable expression across the experimental groups (Supplementary Table 2 and 3).

2.11. miRNA transfection

For miRNA transfection experiments, SH-SY5Y (human bone marrow-derived neuroblastoma) cells were seeded in 24-well plates at a concentration of 8×10^4 cells/well and transfected with 500 ng of miRVec-30b-5p, miRVec-101a-3p or an empty vector. Transfections were performed in triplicate using Lipofectamine 2000 transfection reagent (Thermo Fisher Scientific, USA) according to the manufacturer's instructions. RNA was extracted following 48h for miRNAs and following 72h for mRNAs. Transfection efficiencies were measured by GFP fluorescence in all cells, indicating a transfection efficiency of >20%.

2.12. Dual luciferase reporter assays

Fragments of ~700 bp from *QKI* 3′UTR, spanning the presumed miRNA-binding sites, were cloned, downstream of the Renilla luciferase reporter under the control of T7 promoter of the psiCHECK-2 plasmid (Promega, USA), which also contains a firefly luciferase reporter (used as a control) under the HSV-TK promoter. The negative controls of *QKI*, in which miRNA-mRNA binding is abolished, were generated by mutating three nucleotides in the seed binding region of the cloned QKI 3′UTR, using the QuikChange Lightning Site-Directed Mutagenesis Kit (Agilent technologies, USA). For luciferase assays, HEK-293T human cells were transfected using Lipofectamine 2000 transfection reagent. Next, the cells were transfected with 5 ng of psiCHECK-2 plasmid containing the desired 3′UTR, with or without site-directed mutations, and 485 ng miRVec containing the desired pre-miRNA or an empty vector. At 72h following transfection, firefly and Renilla luciferase activities were measured using the Dual Luciferase Reporter assay system kit (Promega, USA) and the LUMIstar Omega Luminometer (BMG Lab-Tech, Germany), according to the manufacturer's recommendations. Renilla luciferase results were normalized to the values of the firefly luciferase. Significant results represent 3 biological replicates.

2.13. Western blotting

Thirty-six raphe nuclei and superior colliculus samples from the 2nd cohort were homogenized in solubilization buffer (50 nM HEPES PH = 7.5, 10 nM NaCl, 10% glycerol, 1% Triton x-100, 1 mM EDTA pH = 8, 1 mM EGTA pH = 8, 1.5 mM MgCl2, 200 μM Na3VO4, and protease inhibitor cocktail 1 diluted 1:100 (Merck by Mercury Ltd., Rosh Ha'ayin, Israel)). Equal amounts of protein from each sample were loaded and resolved by SDS–polyacrylamide gel electrophoresis through 12.5% gel. The gel was electrophoretically transferred to a nitrocellulose membrane in transfer buffer (25 mM Tris, 190 mM glycine, and 10% methanol absolute). Membranes were blocked for 45 min in TBST buffer (0.05 M Tris HCl pH = 7.5, 0.15 M NaCl, and 0.1% Tween 20) with 6% skimmed milk, and blotted overnight with rat anti-MBP antibody (MAB386, Merck), rabbit anti-β-Tubulin (AB108342, Abcam by Zotal Ltd., Tel Aviv. Israel) and mouse anti-QKI (MA5-27651, Thermo Fisher Scientific, USA) in TBST buffer, followed by a secondary antibody linked to horseradish peroxidase, goat anti-rat, goat anti-rabbit, and goat anti-mouse respectively (AP136P, AP132P, AP130P, Sigma-Aldrich, USA). Immunoreactive bands were detected with the enhanced chemiluminescence reagent.

2.14. Transmission electron microscopy (TEM)

Twelve-weeks old mice from the 2nd cohort were deeply anesthetized with isoflurane, transcardially perfused with 15 ml ice-cold PBS solution followed by 15 ml fresh ice-cold fixative solution containing 2.5% glutaraldehyde (G5882, Sigma-Aldrich, USA) + 2% PFA (EMS, PA, USA) in 0.1 M sodium cacodylate buffer (pH 7.4) (C0250, Sigma-Aldrich, USA). Brains were dissected and Raphe nuclei areas were kept in the fixation solution overnight at 4 °C and then moved to a solution containing 2.5% glutaraldehyde, 0.1M cacodylate buffer and Phosphate-buffered saline (PBS) (Biological Industries, Israel). After several washings in PBS, brain tissues were post fixed in 1% osmium tetroxide (OsO4) in PBS for 2 h at 4 °C. Dehydration was carried out in graded ethanol solutions (10 min each; 50, 70, 90 and 2 × 10 min 100%) and embedding in Glycid ether (Serva, Heidelberg, Germany). Ultra-thin sections (approximately 70 nm) were cut, stained with uranyl acetate and lead citrate, mounted on Formvar/Carbon coated grids and were examined in Jeol 1200EX transmission electron microscope (Jeol, Japan). Images were captured using SIS Megaview III and iTEM the Tem imaging platform (Olympus). For quantifying the number of myelinated axons and characterize the g-ratio, ten images were taken from each of three different locations, to cover multiple regions of the Raphe nuclei. For quantifying the g-ratio, approximately 100 myelinated axons per mouse were analyzed, by manually measuring the ratios of the axons diameter and the myelinated axons diameter.

2.15. Statistical analysis

All data was analyzed using GraphPad Prism software v.9 (San Diego, CA, USA). Normality of data distribution was evaluated using the Shapiro-Wilk test; Outliers were detected by the Grubbs test. For behavioral data, each experimental cohort was analyzed independently, as soon as behavioral measurements were finished, to assess effects of treatment and stress. The contribution of stress and citalopram treatment was analyzed using a two-way ANOVA and Tukey corrections for

multiple testing between categories. Continuous variables between two groups were analyzed by the Student's t-test. Continuous variables between more than two groups were analyzed by the One- or Two-way ANOVA tests. P-values <0.05 were considered significant.

3. Results

3.1. Stress and citalopram affect behavior in CUS mice

The first cohort consisted of male C57BL/6 mice (aged 6 weeks at the start) exposed to CUS in order to impose alterations in depressive and anxiety behaviors. These behaviors were measured by the forced swim test (FST). CUS induced a significant decrease in the latency to immobility. These effects were modified by citalopram dosing (Fig. 1A). Two-way ANOVA analysis of the behavioral data revealed significant interaction effects in latency to immobility ($F(1,19) = 9.86$, $p = 0.005$) and significant effects of CUS ($F(1,19) = 16.89$, $p = 0.0006$) and treatment ($F(1,19) = 4.45$, $p = 0.048$). Significant differences were found between the control group and all the other groups (control/vehicle; $p = 0.008$, stress/vehicle; $p = 0.0004$ and stress/treatment; $p = 0.002$), though stress/vehicle and stress/treatment groups did not differ significantly. Significant differences were not observed in the total inactive time across the four groups (Fig. 1B).

Based on the trend seen in the first cohort, a second, larger cohort was established, which also consisted of 6-week-old mice exposed to CUS, citalopram or both, for 6 weeks. Alterations in depressive and anxiety behaviors in this cohort were measured by the FST and the elevated plus maze (EPM) tests. Two-way ANOVA analysis of the FST behavioral data revealed a significant effect of treatment on latency to immobility ($F(1,43) = 4.24$, $p = 0.045$), and CUS induced a decrease in latency to immobility (Fig. 1C). Two-way ANOVA analysis of the behavioral data revealed interaction effects in the total inactive time ($F(1,43) = 5.81$, $p = 0.020$) and an effect of treatment on the total inactive time ($F(1,43) = 4.42$, $p = 0.041$). Specifically, the inactive duration was increased in the stress/vehicle group compared to the stress/treatment group ($p = 0.016$) (Fig. 1D). Two-way ANOVA analysis of the EPM behavioral data revealed significant interaction effects on the total distance moved ($F(1,43) = 13.82$, $p = 0.0006$); a larger distance was moved in the stress/treatment group than in the stress/vehicle group ($p = 0.001$) (Fig. 1E). Analysis of the time in the EPM open arms revealed significant interaction effects ($F(1,43) = 7.152$, $p = 0.010$); the time in open arms was lower in the stress/vehicle group than in the control/vehicle or stress/treatment groups ($p = 0.001$ and $p = 0.021$, respectively) (Fig. 1F). Both FST and EPM indicated that citalopram attenuated the effects of CUS.

3.2. Stress and citalopram affect brain diffusivity

To examine changes in brain white matter we used MRI-DTI scans. This revealed lower FA in stressed mice than in control mice or stressed mice treated with citalopram. These results may indicate axonal degeneration, demyelination or less dense axonal packing in stressed mice brains. Comparing control and stressed mice (Fig. 2B) showed a significant ($p < 0.05$) effect of stress on FA in five regions, including the RN area (−28%), brain stem area (−19%), retro-spinal cortex (−30%), corpus callosum (−24%) and caudate-putamen (−23%). Comparing stressed mice to stressed mice treated with citalopram showed a significant ($p < 0.05$) effect of stress in six regions, including the RN area (−30%), brain stem area (−21%), corpus callosum (−23%), caudate-putamen (−28%), dentate gyrus (−32%) and globus pallidus (−24%).

MRI-DTI also revealed lower axial diffusivity in stressed mice than in stressed mice treated with citalopram (Fig. 2D), indicating axonal injury. The effect of stress was significant ($p < 0.05$) in three regions, including the RN area (−12%), thalamus (−13%) and caudate-putamen (−13%).

T2 relaxation images were used to assess volumetric changes in the brain following stress or citalopram treatment. Neither of them significantly affected the examined brain region volumes.

3.3. Stress and citalopram alter miR-30b-5p and miR-101a-3p expression in the raphe nucleus

As we were interested in changes in the serotonergic center of the brain, twelve raphe nucleus (RN) and twelve superior colliculus (SC, *i.e.* control area) RNA samples from the first cohort were sent for miRNA profiling via the NanoString platform. We used principal component analysis (PCA) to assess whether global miRNA expression can distinguish between the four mouse groups in each tissue. PCA for SC revealed no distinction between the groups (data not shown). However, PCA for RN distinguished stress/citalopram samples from the other groups; and mildly distinguished between the three other groups (Supplementary Fig. S1). To evaluate whether a miRNA-based risk classifier pattern can be identified, we compared miRNA expression between the groups (control vs. stress, stress vs. stress/citalopram). Many miRNAs were differentially expressed between the groups; and for several miRNAs whose responses to stress and to stress/citalopram were inversely correlated, statistical significance ($p < 0.05$) was shown (Fig. 3A and B). The two miRNAs (miR-30b-5p and miR-101a-3p) with the most significant change were selected for further evaluation.

Real-time PCR was conducted to validate the results, utilizing 11 additional samples from the first cohort that had not been analyzed by the NanoString assay. One-way ANOVA analysis for miR-30b-5p and miR-101a-3p verified that these miRNAs demonstrated the same trend as seen in the NanoString assay: reduced expression following stress and increased expression following stress and citalopram treatment (miR-101a-3p, $p = 0.020$, and miR-30b-5p, $p = 0.026$) (Fig. 3C).

3.4. miR-30b-5p and miR-101a-3p target Qki

Next, we searched for mouse genes that were targeted by both miRNAs. For this purpose, we considered genes as miRNA targets if they were predicted as a target-gene by at least three of four established prediction tools: Target Scan (TargetScanHuman 8), Diana (DIANA TOOLS), miRDIP (Tokar et al., 2018) and Pita (Lab). This resulted in four target-genes for both miR-30b-5p and miR-101a-3p: *Cpeb3*, *Fndc3a*, *Edem3* and *Qki*. The expression levels of the mRNAs of all four genes were tested in the RN tissue by qPCR. *Cpeb3*, *Fndc3a* and *Edem3* showed no significant change (Supplementary Fig. S2). Only *Qki* showed an effect of treatment ($p = 0.0006$); expression levels were inversely correlated with miRNAs in both the stress and stress/citalopram groups ($p = 0.0003$) (Fig. 4A).

To validate the predicted interaction of miR-30b-5p or miR-101a-3p with *Qki*, we quantified the levels of the relevant mRNA after transfection of each miRNA. Two miRNA vectors that expressed miRNA of miR-30b-5p or miR-101a-3p were transfected into the SH-SY5Y cell line for 72 h. Real-time PCR reactions that were carried out on each transfectant revealed the three-fold overexpression of miR-30b-5p, and the 1.5-fold overexpression of miR-101a-3p ($p = 0.006$ and $p = 0.040$, respectively, Fig. 4B). Further, overexpression of miR-30b-5p and miR-101a-3p reduced *Qki* levels by 23% and 12%, respectively ($p = 0.014$ and $p = 0.030$, respectively, Fig. 4C).

To demonstrate the direct functional regulation and binding of miR-30b-5p or miR-101a-3p to *Qki*, a luciferase reporter assay was conducted. Negative controls were generated by performing site-directed mutagenesis reactions that resulted in changes of three nucleotides of the respective 3′UTR miRNA-binding sites of *Qki* in the seed region (Fig. 4D). After 72 h of co-transfection of *Qki* 3′UTR construct and miRNA vector plasmid in HEK-293T cells, Renilla luciferase and firefly luciferase expression was measured. Fig. 4E shows that transfection of plasmids containing the wild-type 3′UTR of *Qki* resulted in lower luciferase activity than that observed following transfection of plasmids containing the mutant 3′ UTR (luciferase activity was reduced to 0.66

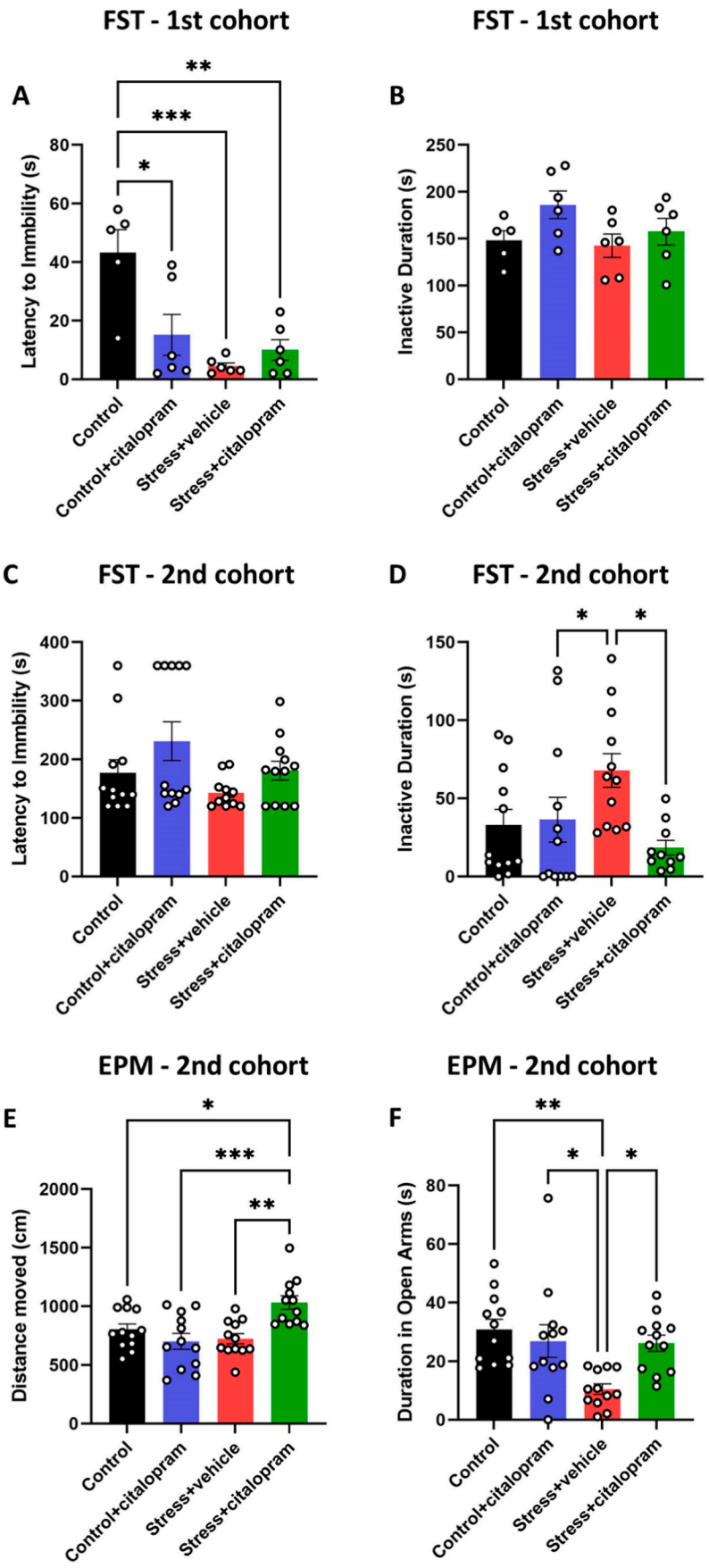

(caption on next page)

Fig. 1. CUS exposed mice display depressive-like and anxiety-like behaviors in the forced swim test (FST) and the elevated plus maze (EPM). (A) latency to immobility and (B) inactive duration in the FST for the first cohort. (C) latency to immobility and (D) inactive duration in the FST for the second cohort. (E) distance moved and (F) duration in the open arms in the EPM for the second cohort. The data are shown as means ± SEM. *$p < 0.05$, **$p < 0.01$, ***$p < 0.001$. Two-way ANOVA test. (A–B) n = 5 control, n = 6 per each of the other groups. (C–F) n = 12 per each of the groups. S, seconds; cm, centimeter.

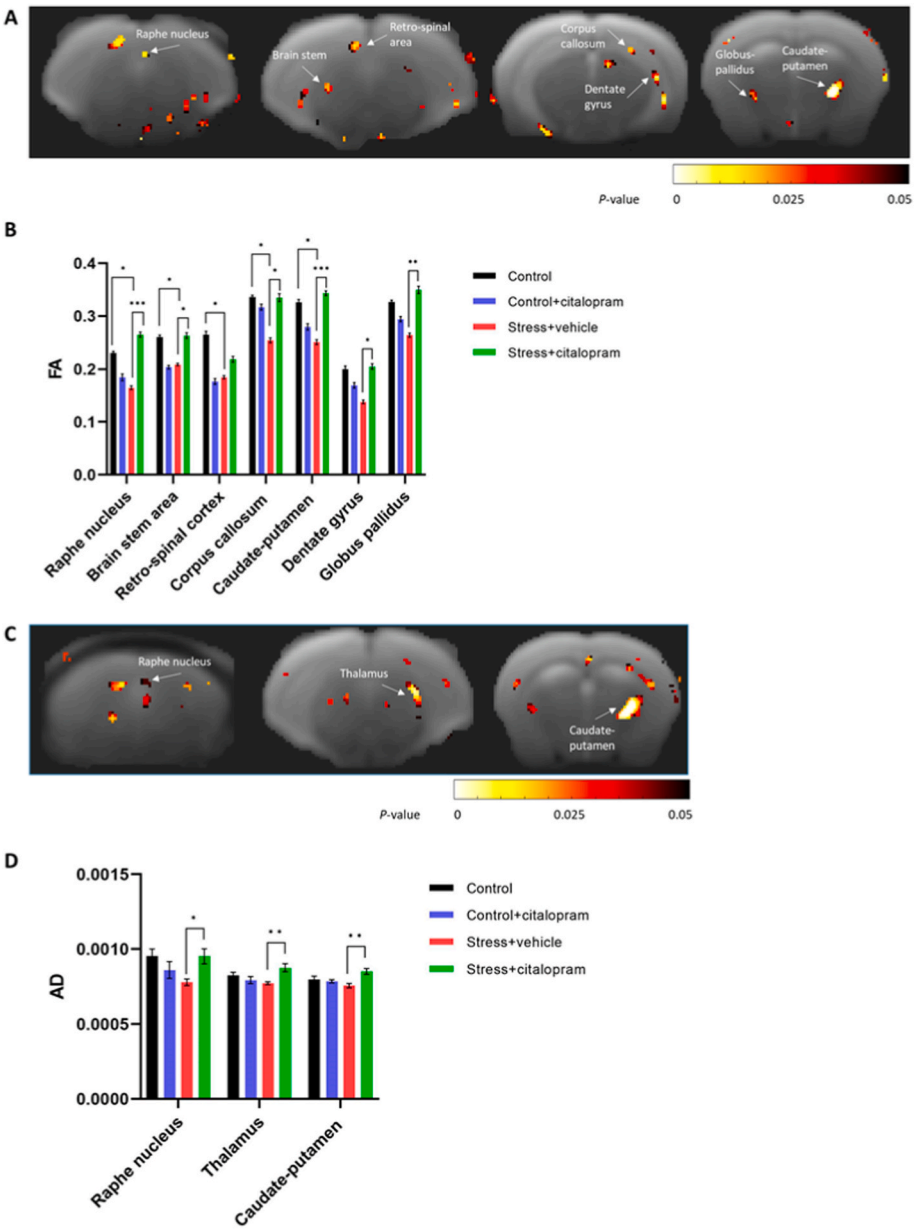

Fig. 2. Voxel-based analysis of MRI-DTI. (A) MRI-DTI brain FA maps comparing between control and stressed mice (two left brains) and between stressed mice and stressed mice treated with citalopram (two right brains). (B) Analysis of fractional anisotropy between all four groups. (C) MRI-DTI brain AD maps between stressed mice and stressed mice treated with citalopram. (D) Analysis of axial diffusivity between all four groups. (A,C) Statistically significant ($p < 0.05$) clusters are overlaid on coronal maps (posterior to anterior, from left to right). The red-yellow color bar indicates the degree of significance (p-value). (B,D) The data are shown as means ± SEM. *$p < 0.05$, **$p < 0.01$, ***$p < 0.001$. One-way ANOVA test. n = 12 per each group.

and 0.63 relative to mutant levels, by miR-30b-5p and miR-101a-3p, $p = 0.004$ and $p = 0.013$, respectively).

3.5. Correlation between Qki and Mbp in the mouse raphe nucleus

AS *Qki* is expressed in oligodendrocytes and involved in myelination processes and their maintenance (Klempan et al., 2009b; Ebersole et al., 1996; Zhou et al., 2020), we looked for myelin-related genes that might be affected by *Qki*. The tested genes were *Cnp*, *Plp1*, *Mag* and *Mbp*. *Cnp*, *Plp1* and *Mag* showed no significant effect of CUS (Supplementary Fig. S3). In contrast, myelin basic protein (*Mbp*) showed significantly decreased mRNA expression levels in the stress condition, and increased levels in the stress and treatment condition ($p = 0.001$). The expression levels of *Mbp* were inversely correlated to *Qki* (stress/vehicle *Qki* vs. *Mbp*; $p < 0.0001$) (Fig. 5A).

Thirty-six raphe nuclei samples from the second cohort were used to investigate changes in protein levels. Compared to stressed mice that were not treated with citalopram, stressed mice that were treated

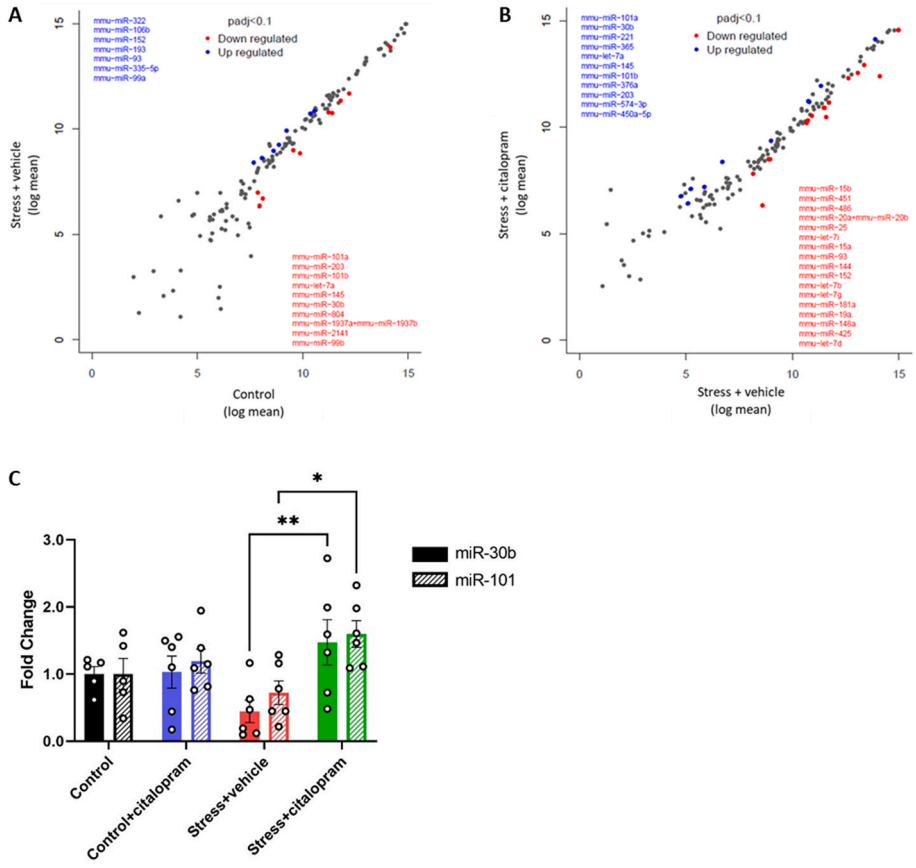

Fig. 3. miRNA expression analysis following 6 weeks of CUS in mice. Log mean expressions of 302 microRNAs that passed quality control filters of NanoString analysis, compared between (A) the stress/vehicle and the control groups and (B) the stress/citalopram and the stress/vehicle groups. Each dot represents a specific miRNA. Red dots represent miRNA with significant downregulated differential expression. Blue dots represent miRNA with significant upregulated differential expression. (C) Real-time qPCR analysis of miR-30b-5p and miR-101a-3p. (C) The data are shown as means ± SEM. *$p < 0.05$, ***$p < 0.001$. One-way ANOVA. (A–B) n = 3 per each mouse group, (C) n = 5 control, n = 6 per each of the other mouse groups.

showed significantly lower ($p = 0.044$) QKI protein expression (Fig. 5B). Although not significant ($p = 0.209$), the opposite trend was shown for MBP protein expression, namely lower expression following stress, and higher expression following citalopram treatment.

As previous studies emphasized the involvement of the nucleic isoform of *Qki*, which includes exon 8 (*Qki*-5), in affecting levels of *Mbp* in oligodendrocytes (Larocque et al., 2002), we tested the level of this isoform in our samples. Although not statistically significant, a trend was seen by which levels of *Qki*-5 were higher in stressed mice, and lower in stressed mice treated with citalopram (Fig. 5D). To ensure that these changes were specific for the *Qki*-5 isoform, levels of the cytoplasmic isoform *Qki*-7 (which includes exon 7) were tested as well. The level of *Qki*-7 was higher in control mice than in control mice treated with citalopram ($p = 0.034$); however, *Qki*-7 levels were similar between stressed mice and stressed mice treated with citalopram (Fig. 5E).

3.6. Unchanged mRNA or protein levels in the mouse superior colliculus (SC)

Following the original NanoString analysis, which showed no change in miRNA expression following stress or citalopram treatment in the SC tissue, we sought to examine mRNA and protein expression for *Qki* and *Mbp*. SC tissue from stressed mice showed similar mRNA and protein expression levels *of Qki* and *Mbp* to those of control mice. SC tissue from stressed mice treated with citalopram showed similar expression levels of *Mbp* mRNA and protein to those of control mice. *Qki* mRNA expression was significantly higher in the stressed mice than in the stressed mice that were treated ($p = 0.020$) (Supplementary Fig. S4A). However, no such difference was observed in the expression of *Mbp* mRNA, or in QKI and MBP proteins (Supplementary Fig. S4B).

3.7. CUS impairs myelin ultrastructure

We next investigated whether the abovementioned molecular deficits affect myelin structure in CUS mice. Analysis of myelin ultrastructure (Fig. 6A) revealed a significantly decreased *g*-ratio, a parameter used for assessment of axonal myelination, for stressed mice compared to control mice, and compared to stressed mice treated with citalopram ($p < 0.0001$ for both comparisons). This indicates increased myelin thickness in stressed mice. However, in images of the axon ultrastructure (Fig. 6B), the myelin diameter of axons of stressed mice was not thicker. Notably, the myelin sheaths in these axons were less compressed together, with gaps formed between them. Citalopram treatment restored normal compacting of the myelin sheaths.

4. Discussion

Chronic stress is well-established as a common trigger for the onset of depressive symptoms (McGonagle and Kessler, 1990; Iñiguez et al., 2014; Zhu et al., 2014), via its effect on the hypothalamic pituitary adrenal axis (Gold, 2015; Hammen, 2005). Chronic stress can also lead to changes in brain function and morphology (Pandya et al., 2012; Schoenfeld and Gould, 2012; Woo et al., 2021; Disner et al., 2011), which are neurological aspects of MDD that are not easily accessible for molecular studies in living humans. Abundant studies in both humans and rodents showed that miRNA expression profiles are altered during

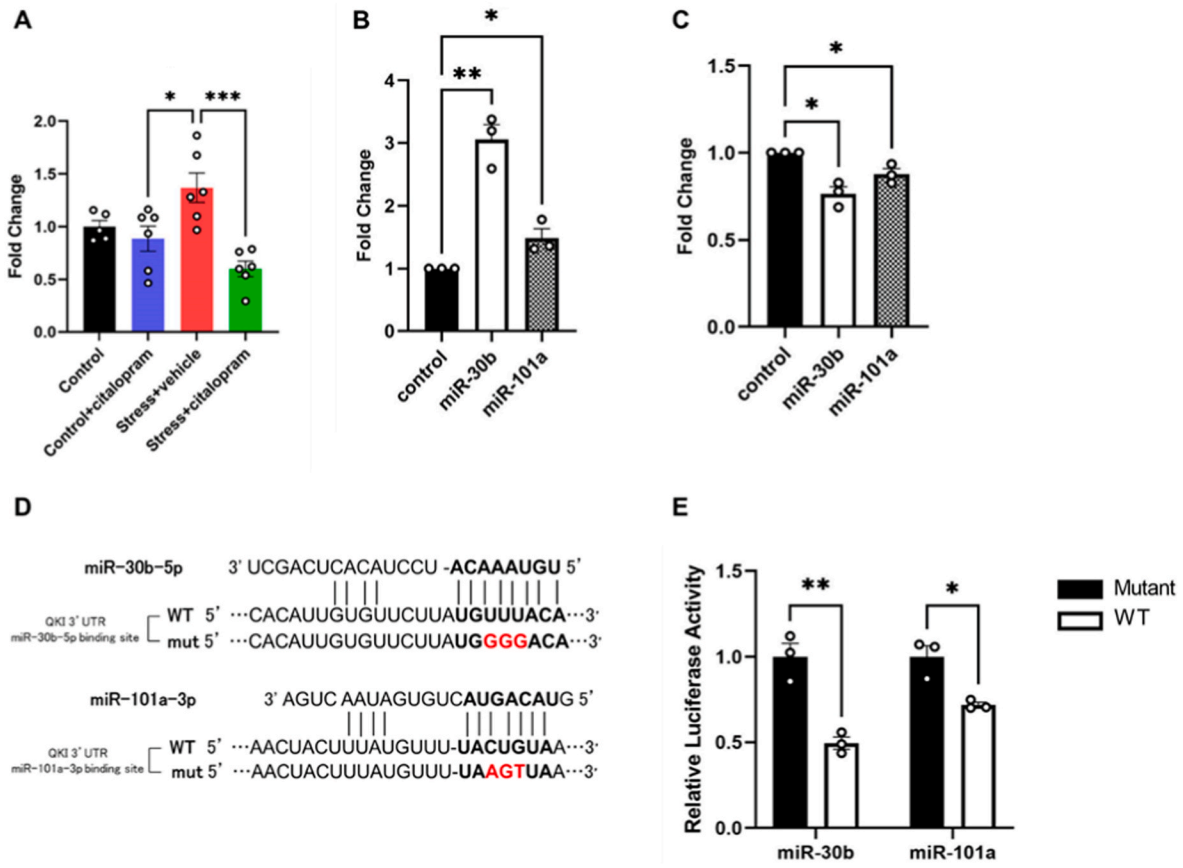

Fig. 4. miR-30b-5p and miR-101a-3p directly regulate *Qki* mRNA. (A) *Qki* expression profile assessed by RT-qPCR. Significantly increased expression levels of *Qki* mRNA in RN of stressed mice compared to stressed and treated mice. (B) Real-time PCR analysis of miRNA following two repeated 24h transfections and of (C) *QKI* mRNA expression following 72h of the indicated miRNA transfection relative to a control plasmid transfection, in the SH-SY5Y cell line. (D) Sequences of the mature miR-30b-5p and miR-101a-3p and the Renilla/firefly luciferase psiCHECK2 constructs (WT and mutant) under the regulation of *QKI* 3′UTR, around the miR-30b-5p and miR-101a-3p binding sites. The miR-mRNA binding sites are shown in bold. Mutated nucleotides are shown in red. (E) Significantly higher luciferase activity levels of the mutated *QKI* 3′UTR construct, 72h following transfection with miR-30b-5p or miR-101a-3p in HEK-293T cells, compared to the activity levels of the WT luciferase construct. The data are shown as means ± SEM. $*p < 0.05$, $**p < 0.01$, $***p < 0.001$. (A) One-way ANOVA (B–D) Two-tailed Student's t-test. (A) n = 5 control, n = 6 per each of the other mouse groups (B–D) n = 3. WT, wild type. Mut, Mutant.

chronic stress (Lekman et al., 2008; Volk et al., 2016; Khandelwal et al., 2019), and that dysregulation of their levels may affect the expression of genes related to the etiology of MDD (Serafini et al., 2014a; Dwivedi, 2011; Garbett et al., 2015).

The monoamine hypothesis of depression relies on the conception that SSRIs relieve depression symptoms mainly via blocking SERT (van Praag et al., 1987; Price et al., 1990). The delay of at least three weeks in relief from MDD symptoms led to the suggestion that alleviating depressive symptoms involves synaptogenesis and neurogenesis (Eisch and Petrik, 2012; Bambico et al., 2013; Mateus-Pinheiro et al., 2013; Oved et al., 2013). Moreover, recent studies show no support for, and even refute, the idea that depression is caused by lowered serotonin levels or less effective serotonin signaling (Moncrieff et al., 2022; Albert et al., 2012; Albert and Benkelfat, 2013; Kendrick and Collinson, 2022). This study focused on the RN, which consist of clusters of serotonergic neurons (Hornung, 2003) that project to almost all cortico-limbic regions and regulate many physiological functions (Michelsen et al., 2008; Hamon and Blier, 2013).

Behavioral tests showed that the CUS protocol applied here resulted in mice that presented depressive-like symptoms, and citalopram alleviated these symptoms. Our MRI-DTI scans showed decreases in FA and axial diffusivity in brains of stressed mice, in areas that included the RN, brain stem, corpus callosum, caudate putamen and thalamus. These changes may suggest axonal degeneration, demyelination or less dense axonal packing in brains of chronically stressed mice. Most studies that examined changes in frontal cortico-limbic areas of individuals with MDD reported lower FA in the corpus callosum, thalamus and caudate (Dillon et al., 2018; Jiang et al., 2017; Tymofiyeva et al., 2017; Yuan et al., 2007). However, a smaller number of MRI-DTI studies reported changes in more posterior brain areas. One such study showed lower FA in the RN of MDD non-remitters (DeLorenzo et al., 2013). Another recent study, which applied TEM, reported reduced volumes of the myelin sheaths in the CA1 region of the hippocampus in rats following four weeks of CUS, but did not examine their RN tissues (xia et al., 2022). Our findings support the importance of the RN in the etiology of MDD, the possible effects of chronic stress on CNS myelin structure, and the tentative role of SSRI treatment in correcting these effects.

Using global miRNA expression analysis, we identified several miRNAs that were differentially expressed between the stress and stress/citalopram groups, while some miRNAs had an inversely correlated response to stress and to stress/citalopram. Two mouse miRNAs, miR-30b-5p and miR-101a-3p, exhibited the most significant reduced expression. This was validated in all the RN samples by real-time qPCR. These findings emphasize that CUS can alter the expression levels of miRNAs in the RN, and that SSRI treatment, such as citalopram, can restore RN expression of these miRNAs to normal levels in the mouse CUS model.

Changes in expression of miR-101a-3p were previously linked to epilepsy (Ghafouri-Fard et al., 2022; Geng et al., 2021), to improving spinal cord injuries (Zhang et al., 2022) and to cerebral injury following

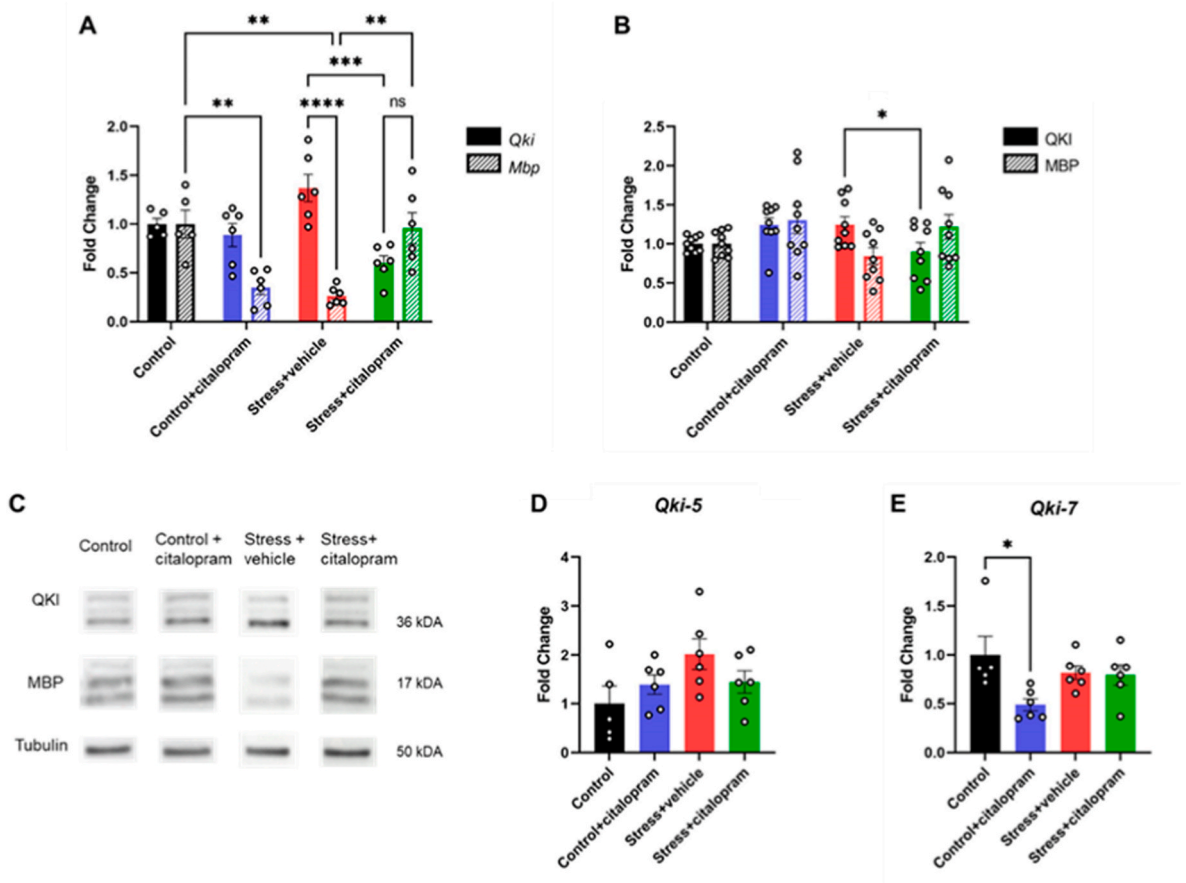

Fig. 5. *Qki* and *Mbp* expression in raphe nuclei (RN) tissue following 6 weeks of CUS in mice. (A) Real-time qPCR analysis of Qki and Mbp mRNA in RN tissues from the four mice groups. (B) Western blot analysis of QKI and MBP protein in all four mice groups. The quantification was done upon normalization to Tubulin housekeeping protein expression. (C) Western blots of MBP and QKI isoform expression levels in the RN of control mice, stressed mice, and treated mice (both control and stressed). (D) Expression levels of *Qki-5* and (E) *Qki-7* isoforms in all four mice groups following PCR amplification. The data are shown as means ± SEM. $*p < 0.05$, $**p < 0.01$, $***p < 0.001$, $****p < 0.0001$. One-way ANOVA test. (A, D-E) n = 5 control, n = 6 per each of the other groups. (B) n = 9 per each group.

ischemia-reperfusion (Fan et al., 2023). Moreover, increased expression levels of miR-101a-3p in the amygdala were found to increase anxiety-like behavior in rodents (Cohen et al., 2017). Most importantly, miR-101a-3p was downregulated in the total plasma of individuals with MDD compared with controls (Homorogan et al., 2021). This suggests the involvement of miR-101a-3p in MDD pathophysiology. Our results support this idea, as miR-101a-3p levels were down-regulated following chronic stress, and were upregulated and restored to normal levels following citalopram treatment.

MiR-30b-5p expression was previously linked mainly to various types of cancer (Zhang et al., 2018; Adam-Artigues et al., 2021; Chen et al., 2022; Wu et al., 2020), as a tumor suppressor. In regard to the CNS, miR-30b-5p was proposed as a free circulating miRNA biomarker in both Alzheimer's and Parkinson's diseases (Dong et al., 2021; Serafin et al., 2015), and its association with MS suggests a role as a general marker of neuro-axonal injury (Ebrahimkhani et al., 2017). Moreover, the expression level of miR-30b-5p, as well as other miR-30 family members, was downregulated in the dentate gyrus of stressed mice (Khandelwal et al., 2019). This suggests that miR-30b-5 may be implicated in a chronic stress-induced depression-like phenotype, by altering neuroplasticity. This may be relevant also to our study.

We identified four protein coding mouse genes that are regulated by both miR-30b-5p and miR-101a-3p, namely: *Cpeb3*, *Fndc3a*, *Edem3* and *Qki*. Only one of them, *Qki*, was inversely correlated to both miRNAs under both the stress and the stress/citalopram conditions. *Qki* (quaking gene) is highly expressed in brain tissue, and is involved in oligodendrocyte and myelination processes (Ebersole et al., 1996). A specific known mutation in this gene results in severe deficits in myelin, a deficiency that is more pronounced in the brain than in the spinal cord or the peripheral nervous system (Friedrich, 1974). *Qki* is an RNA-binding protein with a number of isomers, which regulates pre-mRNA splicing, export of mRNAs from the nucleus, protein translation and mRNA stability (NCBI. QKI). *Qki* was shown to affect RNA processing of the genes encoding *Mbp* and *Mag* in oligodendrocytes (Larocque et al., 2002; Li et al., 2000).

Our study, using luciferase assays, revealed the direct regulation of *Qki* by both miR-30-5p and miR-101a-3p. Furthermore, we showed that reduced *Qki* expression, by 23% and 12% (by miR-30b-5p and miR-101-3p, respectively). In contrast, expression of miR-30b-5p and miR-101a-3p was increased (by 3-fold and 1.5-fold, respectively) following miRNA transfection of both miRNAs in SH-SY5Y cells. These findings may suggest the involvement of *Qki*, and hence its *Mbp* mRNA target, in dysregulated myelination processes, subsequent to downregulation of miR-30b-5p and miR-101a-3p.

In Qk^{v} (quaking viable) mice, which carry a certain mutation in *Qki*, the rate of synthesis of MBP by oligodendrocytes was shown to be unaffected (Brostoff et al., 1977), but the level of *Mbp* mRNA was reduced (Li et al., 2000). This suggests that the QKI protein might regulate myelination in the CNS via alternative pathways to oligodendrocyte differentiation. Oligodendrocytes of wild-type mice express three major *Qki* mRNA isoforms, encoding *Qki*-5, *Qki*-6 and *Qki*-7. While *Qki*-6 and *Qki*-7 are cytoplasmic, *Qki*-5 is nucleic (Larocque et al., 2002). QKI RNA binding proteins bind a short element in the *Mbp* 3′UTR. Elevated levels of *Qki*-5 were shown to cause nuclear export defects of *Mbp* mRNA in

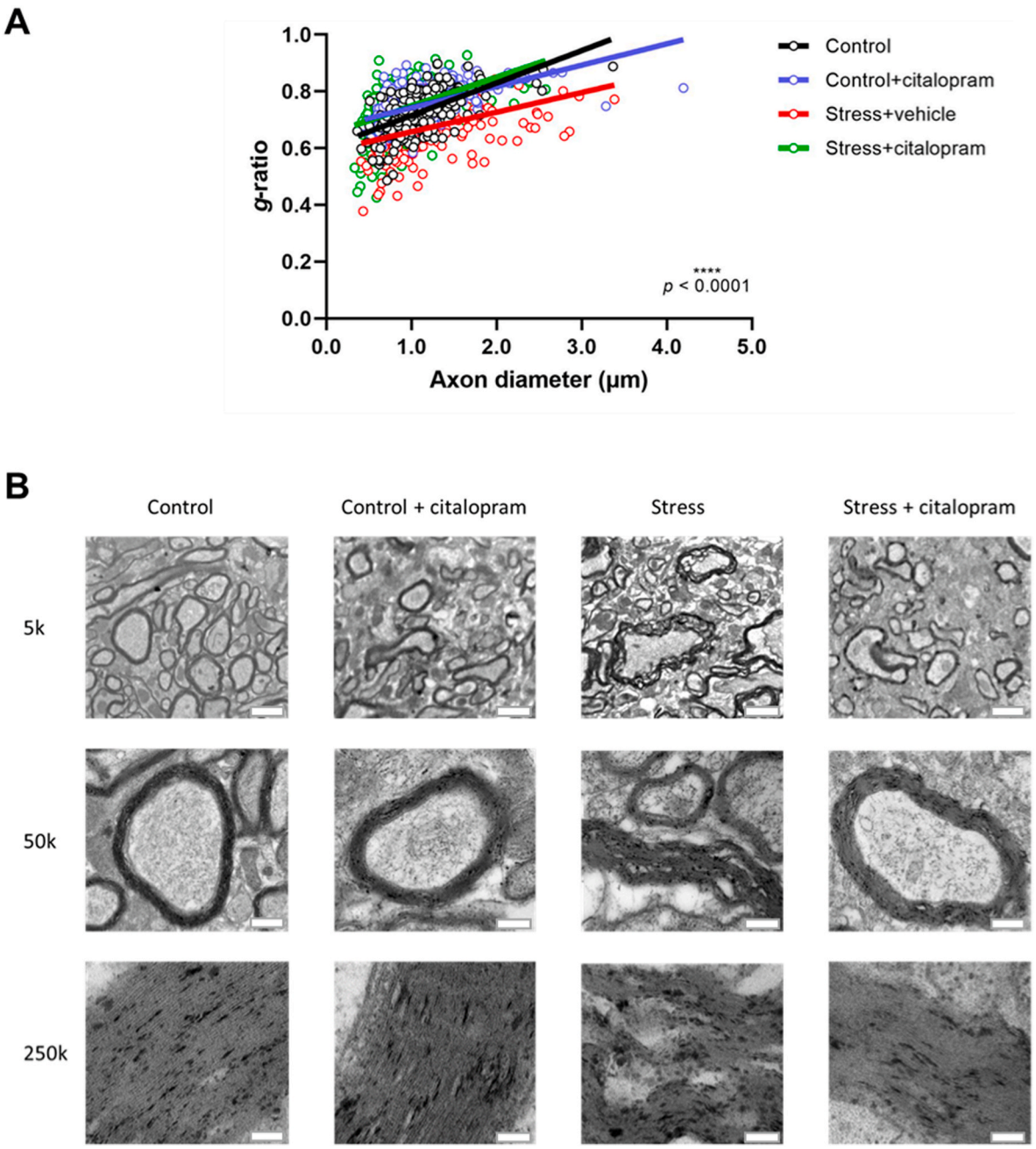

Fig. 6. CUS mice showed impaired myelin ultrastructure. (A) The g-ratio of myelinated axons in the RN of the four mice groups. (B) Representative images of myelin ultrastructure in the RN of the four groups. Scale bars: upper = 5 μm; middle = 500 nm; lower = 100 nm ****$p < 0.0001$. One-way ANOVA. A. n = 203 axons from two control mice, n = 285 axons from three control mice treated with citalopram, n = 216 axons from two stressed mice, n = 274 axons from three stressed mice treated with citalopram.

oligodendrocytes, leading to lower levels of MBP protein levels, especially at distal branching sites (Larocque et al., 2002).

Our findings suggest similar results, in the context of stress and SSRI treatment. Stressed mice that showed higher RN levels of *Qki* mRNA, showed lower RN levels of *Mbp* mRNA. This effect was reversed under citalopram treatment. Furthermore, the same effects were seen in protein levels of both QKI and MBP. Expression levels of the *Qki*-5 isoform were higher, though without statistical significance, in the RN of stressed mice than in citalopram treated mice, while *Qki*-7 isoform levels were similar for both groups. This suggests that nuclear retention of *Mbp* mRNA by *Qki*-5 might be the reason for myelin deficits in chronically stressed mice.

Interestingly, *Mbp* mRNA levels were significantly lower in control mice treated with citalopram, than in control mice that were not treated, despite the lack of difference in the expression levels of miR-30b-5p, miR-101a-3p or *Qki* mRNA. The expression level of *Qki*-7 isoform was also lower in the control group that was not treated; however, MBP protein levels did not differ between the control groups. One explanation might be that citalopram treatment of non-stressed mice might cause changes in *Mbp* mRNA levels, but an alternative mechanism prevents these changes from affecting the MBP protein level.

To verify that the observed changes were unique to the RN, we also tested mRNA and protein levels of *Qki* and *Mbp* in the SC, a tissue located above the RN, but involved in a completely different circuit (Basso et al., 2021). Neither mRNA or protein expression levels of *Qki* or *Mbp* differed in this tissue between stressed mice and stressed mice treated with

citalopram. These results imply the specific and unique impact of SSRIs on the RN in treating myelination defects through regulated expression of *Qki*.

To investigate the effect of the observed molecular changes on CNS myelin structures, we performed TEM imaging and analysis of the RN tissue from mice of all four groups. The *g*-ratio of axons from stressed mice was significantly lower than that of control mice, or than stressed mice that were treated with citalopram. As a lower *g*-ratio represents higher myelin thickness in specific axons, the *g*-ratio indicated thicker myelin in stressed mice than in control mice, or than stressed mice treated with citalopram. However, images of the axons revealed a different picture, in which myelin sheaths of axons in stressed mice were not compressed and gaps appeared between the myelin sheaths. This effect did not present in myelin of axons from control mice or from stressed mice treated with citalopram. These gaps cause the myelinated axons to show "thicker" myelin. MBP is known as essential for compaction of adjacent membrane surfaces into dense myelin stacks (Stadelmann et al., 2019). This is primarily based on the observation of loosely compacted myelin in *shiverer* mice that carry a mutation in the MBP gene (Roach et al., 1983, 1985). Nuclear retention of *Mbp* that leads to less MBP protein in the distal areas of oligodendrocyte branching sites seems to be the cause of the loosely compacted myelin sheaths observed in mice following the CUS protocol. Properly compacted myelin in RN axons of stressed mice treated with citalopram suggests a mechanism by which SSRIs can affect and ameliorate depression, by directly affecting oligodendrocytes and correcting myelin deficits, and not only through serotonin levels and reuptake.

Based on our findings, we suggest a role for miR-30b-5p and miR-101a-3p, and their target gene *Qki,* in the antidepressant mode of action of SSRI therapeutics, such as citalopram. Our hypothesis (Fig. 7) relies on the knowledge that SSRIs block the reuptake of serotonin by pre-synaptic SERT, but that depression symptoms are not immediately alleviated (van Praag et al., 1987), and that *Qki* is highly expressed in brain oligodendrocytes, and affects myelination processes (Ebersole et al., 1996; Bockbrader and Feng, 2008; Wu et al., 2001; Zhao et al., 2006). We therefore suggest that chronic stress affects the RN, which causes reduced expression of miR-30-5p and miR-101a-3p, via yet unknown pathways. This in turn causes the overexpression of *Qki*, one of their gene targets, specifically isoform *Qki*-5, which induces nuclear retention of *Mbp* mRNA, and lower levels of MBP protein at distal areas of the oligodendrocytes. As the MBP protein is required for correct myelin ensheathing of axons (Larocque et al., 2002), this leads to insufficient compacting of the myelin sheaths. These deficits in oligodendrocyte and myelin function may disturb signal transduction from the RN along their projections to further limbic system tissues, which may, in turn, instigate depressive symptoms.

A second aspect of our hypothesis suggests that SSRI treatment causes increased transcription of RN oligodendrocytes miR-30b-5p and miR-101a-3p, which in turn restores lower levels of *Qki* mRNA and protein. This results in reduced nuclear retention of *Mbp* by *Qki*-5, which enables sufficient amounts of *Mbp* mRNA to move from the oligodendrocyte's nucleus to the cytoplasm, and allows normal levels of MBP protein at distal areas. Adequate amounts of MBP protein enhance myelin repair processes, specifically correcting stress-induced dense compacting of myelin sheaths. This aids in recovering correct signal transduction in the projections that ascend from the RN, and amelioration of depressive symptoms instigated by chronic stress of affected individuals.

Antidepressant drugs were suggested to act by affecting neurogenesis, synaptogenesis and synaptic plasticity (Price et al., 1990; Gelenberg, 2010; Eisch and Petrik, 2012; Hanson et al., 2011; Serafini et al., 2014b). Our hypothesis adds to this knowledge, by suggesting the involvement of antidepressant drugs in myelination processes of RN neuronal axons. Our work showed that *Qki*, a gene expressed in oligodendrocytes that interferes with proper myelination by inhibition of extra-nuclear transport of *Mbp* mRNA to the cytosol, is regulated by both miR-30b-5p and miR-101a-3p. Indeed, under chronic stress, both these miRNAs were downregulated and *Qki* was upregulated. This resulted in impaired MBP protein levels and an adverse effect on RN neuron myelination. Consistent with this tentative mechanism of action, SSRI

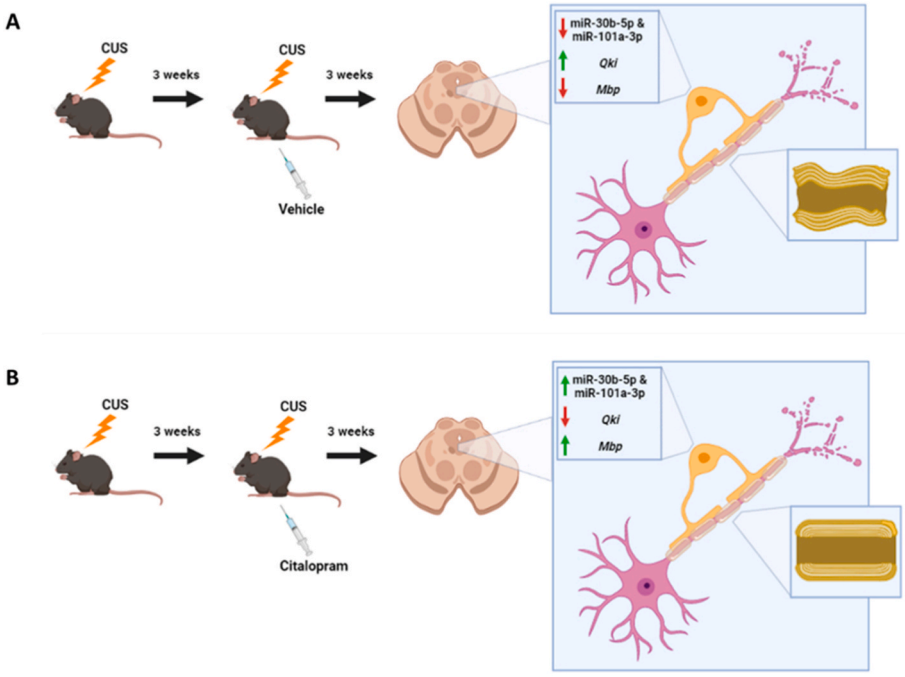

Fig. 7. A hypothetical model depicting a potential role of miR-30b-5p and miR-101a-3p, and their target gene *Qki,* in the mode of action of SSRIs in MDD. (A) Under CUS conditions for 6 weeks, miR-30b-5p and miR-101a-3p are downregulated in the raphe nucleus (RN). This results in higher expression of *Qki*, which in turn causes lower levels of *Mbp* mRNA and protein. This causes looser compacting of myelin sheaths of RN neurons. (B) Under CUS conditions for 6 weeks and citalopram treatment for 3 weeks, miR-30b-5p and miR-101a-3p are up-regulated in the RN, resulting in lower expression of *Qki*. This in turn causes higher levels of *Mbp* mRNA and protein. The latter results in denser and correct compacting of myelin sheaths of RN neurons. Created with BioRender.com.

treatment affects oligodendrocytes and upregulates the expression of both the abovementioned miRNAs. This in turn downregulates *Qki* and restores normal levels of *Mbp* mRNA and myelin functions. Our hypothesis concurs with studies that showed no support for the idea that depression is caused by lowered serotonin levels or activity (Moncrieff et al., 2022; Albert et al., 2012; Albert and Benkelfat, 2013; Kendrick and Collinson, 2022). Moreover, it corroborates explanations of the delay, by weeks to months, in the antidepressant response to SSRIs, and in the restoration of normal levels of MBP protein at distal areas of the oligodendrocyte in conjunction with the re-compacting of the myelin sheaths (Gelenberg, 2010; Rayner et al., 2011; Cipriani et al., 2012; Simons and Nave, 2016). In addition, our hypothesis presents a new explanation to the mechanism underlying the antidepressant response to SSRIs.

In conclusion, we detected specific gene and miRNA changes in RN of stressed mice, who were or were not treated with citalopram. Moreover, we identified changes in myelin compaction in RN of stressed mice. Therefore, we propose miR-30b-5p and miR-101a-3p, together with *Qki,* as SSRI response biomarkers in the RN of mouse MDD model. Further studies are required for validating our hypothesis on dysfunctional axon myelination in MDD, and its correction by SSRI drugs. Expanding our knowledge on axon myelination deficits in MDD may open new venues for developing oligodendrocyte-targeted antidepressant therapeutics, possibly including miRNA mimics.

Author statement

We hereby submit our revised manuscript JPSYCHIATRRES-D-23-00977, entitled: 'Impaired myelin ultrastructure is reversed by citalopram treatment in a mouse model for major depressive disorder, by Israel-Elgali et al.

The material presented in this paper is an original research, has not been previously published and has not been submitted for publication elsewhere while under consideration.

Declaration of competing interest

The authors declare that the research was conducted in the absence of any commercial or financial relationships that could be construed as a potential conflict of interest.

Acknowledgments

The authors thank Cindy Cohen for editorial assistance. This study was supported by the Israel Ministry of Science grant number 3-17928 in the framework of the ERA PerMed project "Artificial intelligence for personalised medicine in depression (ArtiPro)".

Appendix A. Supplementary data

Supplementary data to this article can be found online at https://doi.org/10.1016/j.jpsychires.2023.09.012.

References

Adam-Artigues, A., Garrido-Cano, I., Simón, S., Ortega, B., Moragón, S., Lameirinhas, A., et al., 2021. Circulating miR-30b-5p levels in plasma as a novel potential biomarker for early detection of breast cancer. ESMO Open 6 (1), 100039.

Albert, P.R., Benkelfat, C., 2013. The neurobiology of depression–revisiting the serotonin hypothesis. II. Genetic, epigenetic and clinical studies. Philos. Trans. R. Soc. Lond. B Biol. Sci. 368 (1615), 20120535.

Albert, P.R., Benkelfat, C., Descarries, L., 2012. The neurobiology of depression–revisiting the serotonin hypothesis. I. Cellular and molecular mechanisms. Philos. Trans. R. Soc. Lond. B Biol. Sci. 367 (1601), 2378–2381.

Aston, C., Jiang, L., Sokolov, B.P., 2005. Transcriptional profiling reveals evidence for signaling and oligodendroglial abnormalities in the temporal cortex from patients with major depressive disorder. Mol. Psychiatr. 10 (3), 309–322.

Bambico, F.R., Belzung, C., 2013. Novel insights into depression and antidepressants: a synergy between synaptogenesis and neurogenesis? In: Belzung, C., Wigmore, P. (Eds.), Neurogenesis and Neural Plasticity [Internet]. Springer, Berlin, Heidelberg. https://doi.org/10.1007/7854_2012_234 [cited 2022 Nov 16]. pp. 243–91. (Current Topics in Behavioral Neurosciences).

Basso, M.A., Bickford, M.E., Cang, J., 2021. Unraveling circuits of visual perception and cognition through the superior colliculus. Neuron 109 (6), 918–937.

Bockbrader, K., Feng, Y., 2008. Essential function, sophisticated regulation and pathological impact of the selective RNA-binding protein QKI in CNS myelin development. Future Neurol. 3 (6), 655–668.

Bradl, M., Lassmann, H., 2010. Oligodendrocytes: biology and pathology. Acta Neuropathol. 119 (1), 37–53.

Brostoff, S.W., Greenfield, S., Hogan, E.L., 1977. The differentiation of synthesis from incorporation of basic protein in quaking mutant mouse myelin. Brain Res. 120 (3), 517–520.

Chen, K., Wang, Q., Liu, X., Wang, F., Yang, Y., Tian, X., 2022. Hypoxic pancreatic cancer derived exosomal miR-30b-5p promotes tumor angiogenesis by inhibiting GJA1 expression. Int. J. Biol. Sci. 18 (3), 1220–1237.

Chwastiak, L.A., Ehde, D.M., 2007. Psychiatric issues in multiple sclerosis. Psychiatr. Clin. 30 (4), 803–817.

Cipriani, A., Purgato, M., Furukawa, T.A., Trespidi, C., Imperadore, G., Signoretti, A., et al., 2012. Citalopram versus other anti-depressive agents for depression. Cochrane Database Syst. Rev. 7. CD006534.

Cohen, J.L., Jackson, N.L., Ballestas, M.E., Webb, W.M., Lubin, F.D., Clinton, S.M., 2017. Amygdalar expression of the microRNA miR-101a and its target Ezh2 contribute to rodent anxiety-like behaviour. Eur. J. Neurosci. 46 (7), 2241–2252.

Commons, K.G., 2020. Dorsal raphe organization. J. Chem. Neuroanat. 110, 101868.

Czéh, B., Fuchs, E., Wiborg, O., Simon, M., 2016. Animal models of major depression and their clinical implications. Prog. Neuro Psychopharmacol. Biol. Psychiatr. 64, 293–310.

Darbelli, L., Choquet, K., Richard, S., Kleinman, C.L., 2017. Transcriptome profiling of mouse brains with qkI -deficient oligodendrocytes reveals major alternative splicing defects including self-splicing. Sci. Rep. 7 (1), 7554.

DeLorenzo, C., Delaparte, L., Thapa-Chhetry, B., Miller, J.M., Mann, J.J., Parsey, R.V., 2013. Prediction of selective serotonin reuptake inhibitor response using diffusion-weighted MRI. Front. Psychiatr. 4, 5.

Depressive disorder (depression) [Internet]. [cited 2023 Apr 7]. Available from: https://www.who.int/news-room/fact-sheets/detail/depression.

DIANA TOOLS [Internet]. 2014 [cited 2022 Dec 2]. DIANA Tools. Available from: http://diana.imis.athena-innovation.gr/DianaTools/index.php.

Dillon, D.G., Gonenc, A., Belleau, E., Pizzagalli, D.A., 2018. Depression is associated with dimensional and categorical effects on white matter pathways. Depress. Anxiety 35 (5), 440–447.

Disner, S.G., Beevers, C.G., Haigh, E.A.P., Beck, A.T., 2011. Neural mechanisms of the cognitive model of depression. Nat. Rev. Neurosci. 12 (8), 467–477.

Dong, Z., Gu, H., Guo, Q., Liang, S., Xue, J., Yao, F., et al., 2021. Profiling of serum exosome MiRNA reveals the potential of a MiRNA panel as diagnostic biomarker for alzheimer's disease. Mol. Neurobiol. 58 (7), 3084–3094.

Dwivedi, Y., 2011. Evidence demonstrating role of microRNAs in the etiopathology of major depression. J. Chem. Neuroanat. 42 (2), 142–156.

Dwivedi, Y., 2013. microRNAs as biomarker in depression pathogenesis. Ann. Psychiatry Ment Health 1 (1), 1003.

D'Sa, C., Duman, R.S., 2002. Antidepressants and neuroplasticity. Bipolar Disord. 4 (3), 183–194.

Ebersole, T.A., Chen, Q., Justice, M.J., Artzt, K., 1996. The quaking gene product necessary in embryogenesis and myelination combines features of RNA binding and signal transduction proteins. Nat. Genet. 12 (3), 260–265.

Ebrahimkhani, S., Vafaee, F., Young, P.E., Hur, S.S.J., Hawke, S., Devenney, E., et al., 2017. Exosomal microRNA signatures in multiple sclerosis reflect disease status. Sci. Rep. 7 (1), 14293.

Eisch, A.J., Petrik, D., 2012. Depression and hippocampal neurogenesis: a road to remission? Science 338 (6103), 72–75.

Fan, L.W., Bhatt, A., Tien, L.T., Zheng, B., Simpson, K.L., Lin, R.C.S., et al., 2015. Exposure to serotonin adversely affects oligodendrocyte development and myelination in vitro. J. Neurochem. 133 (4), 532–543.

Fan, W., Qin, Y., Tan, J., Li, B., Liu, Y., Rong, J., et al., 2023. RGD1564534 represses NLRP3 inflammasome activity in cerebral injury following ischemia-reperfusion by impairing miR-101a-3p-mediated Dusp1 inhibition. Exp. Neurol. 359, 114266.

Fiore, R., Siegel, G., Schratt, G., 2008. MicroRNA function in neuronal development, plasticity and disease. Biochim. Biophys. Acta (BBA) -Gene Regulat. Mech. 1779 (8), 471–478.

Forero, D.A., van der Ven, K., Callaerts, P., Del-Favero, J., 2010. miRNA genes and the brain: implications for psychiatric disordersa. Hum. Mutat. 31 (11), 1195–1204.

Franklin, R.J.M., Ffrench-Constant, C., 2017. Regenerating CNS myelin - from mechanisms to experimental medicines. Nat. Rev. Neurosci. 18 (12), 753–769.

Friedrich, V.L., 1974. The myelin deficit in quaking mice. Brain Res. 82 (1), 168–172.

Garbett, K.A., Vereczkei, A., Kálmán, S., Brown, J.A., Taylor, W.D., Faludi, G., et al., 2015. Coordinated messenger RNA/microRNA changes in fibroblasts of patients with major depression. Biol. Psychiatr. 77 (3), 256–265.

Gelenberg, A.J., 2010. A review of the current guidelines for depression treatment. J. Clin. Psychiatry 71 (7), 26478.

Geng, J., Zhao, H., Liu, X., Geng, J., Gao, Y., He, B., 2021. MiR-101a-3p attenuated pilocarpine-induced epilepsy by downregulating c-FOS. Neurochem. Res. 46 (5), 1119–1128.

Ghafouri-Fard, S., Hussen, B.M., Abak, A., Taheri, M., Jalili Khoshnoud, R., 2022. Aberrant expression of miRNAs in epilepsy. Mol. Biol. Rep. 49 (6), 5057–5074.

Gold, P.W., 2015. The organization of the stress system and its dysregulation in depressive illness. Mol. Psychiatr. 20 (1), 32–47.

Gurwitz, D., 2019. Genomics and the future of psychopharmacology: MicroRNAs offer novel therapeutics. Dialogues Clin. Neurosci. 21 (2), 131–148.
Hakak, Y., Walker, J.R., Li, C., Wong, W.H., Davis, K.L., Buxbaum, J.D., et al., 2001. Genome-wide expression analysis reveals dysregulation of myelination-related genes in chronic schizophrenia. Proc. Natl. Acad. Sci. USA 98 (8), 4746–4751.
Hamidi, M., Drevets, W.C., Price, J.L., 2004. Glial reduction in amygdala in major depressive disorder is due to oligodendrocytes. Biol. Psychiatr. 55 (6), 563–569.
Hammen, C., 2005. Stress and depression. Annu. Rev. Clin. Psychol. 1 (1), 293–319.
Hamon, M., Blier, P., 2013. Monoamine neurocircuitry in depression and strategies for new treatments. Prog. Neuro Psychopharmacol. Biol. Psychiatr. 45, 54–63.
Hanson, N.D., Owens, M.J., Nemeroff, C.B., 2011. Depression, antidepressants, and neurogenesis: a critical reappraisal. Neuropsychopharmacology 36 (13), 2589–2602.
Hasin, D.S., Sarvet, A.L., Meyers, J.L., Saha, T.D., Ruan, W.J., Stohl, M., et al., 2018. Epidemiology of adult DSM-5 major depressive disorder and its specifiers in the United States. JAMA Psychiatr. 75 (4), 336–346.
Hirschfeld, R.M., 2000. History and evolution of the monoamine hypothesis of depression. J. Clin. Psychiatry 61 (Suppl. 6), 4–6.
Homorogan, C., Enatescu, V.R., Nitusca, D., Marcu, A., Seclaman, E., Marian, C., 2021. Distribution of microRNAs associated with major depressive disorder among blood compartments. J. Int. Med. Res. 49 (4), 03000605211006633.
Hornung, J.P., 2003. The human raphe nuclei and the serotonergic system. J. Chem. Neuroanat. 26 (4), 331–343.
Im, H.I., Kenny, P.J., 2012. MicroRNAs in neuronal function and dysfunction. Trends Neurosci. 35 (5), 325–334.
Iñiguez, S.D., Riggs, L.M., Nieto, S.J., Dayrit, G., Zamora, N.N., Shawhan, K.L., et al., 2014. Social defeat stress induces a depression-like phenotype in adolescent male c57BL/6 mice. Stress 17 (3), 247–255.
Jiang, J., Zhao, Y.J., Hu, X.Y., Du, M.Y., Chen, Z.Q., Wu, M., et al., 2017. Microstructural brain abnormalities in medication-free patients with major depressive disorder: a systematic review and meta-analysis of diffusion tensor imaging. J. Psychiatry Neurosci. 42 (3), 150–163.
Joffe, R.T., Lippert, G.P., Gray, T.A., Sawa, G., Horvath, Z., 1987. Mood disorder and multiple sclerosis. Arch. Neurol. 44 (4), 376–378.
Kendrick, T., Collinson, S., 2022. Antidepressants and the serotonin hypothesis of depression. BMJ 378, o1993.
Khandelwal, N., Dey, S.K., Chakravarty, S., Kumar, A., 2019. miR-30 family miRNAs mediate the effect of chronic social defeat stress on hippocampal neurogenesis in mouse depression model [Internet] Front. Mol. Neurosci. [cited 2022 Nov 17];12 https://www.frontiersin.org/articles/10.3389/fnmol.2019.00188.
Klempan, T.A., Sequeira, A., Canetti, L., Lalovic, A., Ernst, C., ffrench-Mullen, J., et al., 2009a. Altered expression of genes involved in ATP biosynthesis and GABAergic neurotransmission in the ventral prefrontal cortex of suicides with and without major depression. Mol. Psychiatr. 14 (2), 175–189.
Klempan, T.A., Ernst, C., Deleva, V., Labonte, B., Turecki, G., 2009b. Characterization of QKI gene expression, genetics, and epigenetics in suicide victims with major depressive disorder. Biol. Psychiatr. 66 (9), 824–831.
Kuhn, S., Gritti, L., Crooks, D., Dombrowski, Y., 2019. Oligodendrocytes in development, myelin generation and beyond. Cells 8 (11), 1424.
Kurokawa, K., Takahashi, K., Miyagawa, K., Mochida-Saito, A., Takeda, H., Tsuji, M., 2021. Activation of 5-HT1A receptor reduces abnormal emotionality in stress-maladaptive mice by alleviating decreased myelin protein in the ventral hippocampus. Neurochem. Int. 151, 105213.
Lab, Segal. microRNA 2007 - Predict your UTR [Internet]. [cited 2022 Dec 2]. Available from: https://genie.weizmann.ac.il/pubs/mir07/mir07_prediction.html.
Larocque, D., Pilotte, J., Chen, T., Cloutier, F., Massie, B., Pedraza, L., et al., 2002. Nuclear retention of MBP mRNAs in the quaking viable mice. Neuron 36 (5), 815–829.
Leemans, A., Jeurissen, B., Sijbers, J., Jones, D.K., 2009. ExploreDTI: a graphical toolbox for processing, analyzing, and visualizing diffusion MR data [cited 2023 Jan 9]. Available from: https://www.semanticscholar.org/paper/ExploreDTI%3A-a-graphical-toolbox-for-processing%2C-and-Leemans-Jeurissen/f92f4418d4a4523a5760414144ecce8ab6472fde.
Lekman, M., Laje, G., Charney, D., Rush, A.J., Wilson, A.F., Sorant, A.J.M., et al., 2008. The FKBP5-gene in depression and treatment response—an association study in the sequenced treatment alternatives to relieve depression (STAR*D) cohort. Biol. Psychiatr. 63 (12), 1103–1110.
Li, Z., Zhang, Y., Li, D., Feng, Y., 2000. Destabilization and mislocalization of myelin basic protein mRNAs in quaking dysmyelination lacking the QKI RNA-binding proteins. J. Neurosci. 20 (13), 4944–4953.
Lim, L.P., Lau, N.C., Garrett-Engele, P., Grimson, A., Schelter, J.M., Castle, J., et al., 2005. Microarray analysis shows that some microRNAs downregulate large numbers of target mRNAs. Nature 433 (7027), 769–773.
Londin, E., Loher, P., Telonis, A.G., Quann, K., Clark, P., Jing, Y., et al., 2015. Analysis of 13 cell types reveals evidence for the expression of numerous novel primate- and tissue-specific microRNAs. Proc. Natl. Acad. Sci. U. S. A. 112 (10), E1106–E1115.
Lopez, A.D., Mathers, C.D., Ezzati, M., Jamison, D.T., Murray, C.J., 2006. Global and regional burden of disease and risk factors, 2001: systematic analysis of population health data. Lancet 367 (9524), 1747–1757.
Mateus-Pinheiro, A., Pinto, L., Bessa, J.M., Morais, M., Alves, N.D., Monteiro, S., et al., 2013. Sustained remission from depressive-like behavior depends on hippocampal neurogenesis. Transl. Psychiatry 3 (1), e210.
McGonagle, K.A., Kessler, R.C., 1990. Chronic stress, acute stress, and depressive symptoms. Am. J. Community Psychol. 18 (5), 681–706.
Michelsen, K.A., Prickaerts, J., Steinbusch, H.W.M., 2008. The dorsal raphe nucleus and serotonin: implications for neuroplasticity linked to major depression and Alzheimer's disease. In: Di Giovann, G., Di Matteo, V., Esposito, E. (Eds.), Progress in Brain Research [Internet], (Serotonin–Dopamine Interaction: Experimental Evidence and Therapeutic Relevance, vol. 172. Elsevier [cited 2022 Nov 17]. pp. 233–64. https://www.sciencedirect.com/science/article/pii/S0079612308009126.
Miguel-Hidalgo, J.J., 2023. Astrocytes as context for the involvement of myelin and nodes of ranvier in the pathophysiology of depression and stress-related disorders. J. Psychiatr. Brain Sci. 8, e230001.
Miguel-Hidalgo, J.J., Hall, K.O., Bonner, H., Roller, A.M., Syed, M., Park, C.J., et al., 2017. MicroRNA-21: expression in oligodendrocytes and correlation with low myelin mRNAs in depression and alcoholism. Prog. Neuro Psychopharmacol. Biol. Psychiatr. 79, 503–514.
Miguel-Hidalgo, J.J., Carter, K., Deloach, P.H., Sanders, L., Pang, Y., 2019. Glucocorticoid-induced reductions of myelination and connexin 43 in mixed central nervous system cell cultures are prevented by mifepristone. Neuroscience 411, 255–269.
Modai, S., Shomron, N., 2016. Molecular risk factors for schizophrenia. Trends Mol. Med. 22 (3), 242–253.
Mohammad-Zadeh, L.F., Moses, L., Gwaltney-Brant, S.M., 2008. Serotonin: a review. J. Vet. Pharmacol. Therapeut. 31 (3), 187–199.
Moncrieff, J., Cooper, R.E., Stockmann, T., Amendola, S., Hengartner, M.P., Horowitz, M. A., 2022. The serotonin theory of depression: a systematic umbrella review of the evidence. Mol. Psychiatr. 1–14.
Nave, K.A., 2010. Myelination and support of axonal integrity by glia. Nature 468 (7321), 244–252.
NCBI. QKI [Internet]. 2023 [cited 2022 Dec 3]. Available from: https://www.ncbi.nlm.nih.gov/gene/9444.
Öngür, D., Drevets, W.C., Price, J.L., 1998. Glial reduction in the subgenual prefrontal cortex in mood disorders. Proc. Natl. Acad. Sci. USA 95 (22), 13290–13295.
Oved, K., Morag, A., Pasmanik-Chor, M., Rehavi, M., Shomron, N., Gurwitz, D., 2013. Genome-wide expression profiling of human lymphoblastoid cell lines implicates integrin beta-3 in the mode of action of antidepressants. Transl. Psychiatry 3, e313.
Pandya, M., Altinay, M., Malone, D.A., Anand, A., 2012. Where in the brain is depression? Curr. Psychiatr. Rep. 14 (6), 634–642.
Pillar, N., Bairey, O., Goldschmidt, N., Fellig, Y., Rosenblat, Y., Shehtman, I., et al., 2017. MicroRNAs as predictors for CNS relapse of systemic diffuse large B-cell lymphoma. Oncotarget 8 (49), 86020–86030.
Price, L.H., Charney, D.S., Delgado, P.L., Heninger, G.R., 1990. Lithium and serotonin function: implications for the serotonin hypothesis of depression. Psychopharmacology 100 (1), 3–12.
Rajkowska, G., Mahajan, G., Maciag, D., Sathyanesan, M., Iyo, A.H., Moulana, M., et al., 2015. Oligodendrocyte morphometry and expression of myelin – related mRNA in ventral prefrontal white matter in major depressive disorder. J. Psychiatr. Res. 65, 53–62.
Rajkowska, G., Legutko, B., Moulana, M., Syed, M., Romero, D.G., Stockmeier, C.A., et al., 2018. Astrocyte pathology in the ventral prefrontal white matter in depression. J. Psychiatr. Res. 102, 150–158.
Rayner, L., Price, A., Evans, A., Valsraj, K., Hotopf, M., Higginson, I.J., 2011. Antidepressants for the treatment of depression in palliative care: systematic review and meta-analysis. Palliat. Med. 25 (1), 36–51.
Roach, A., Boylan, K., Horvath, S., Prusiner, S.B., Hood, L.E., 1983. Characterization of cloned cDNA representing rat myelin basic protein: absence of expression in brain of shiverer mutant mice. Cell 34 (3), 799–806.
Roach, A., Takahashi, N., Pravtcheva, D., Ruddle, F., Hood, L., 1985. Chromosomal mapping of mouse myelin basic protein gene and structure and transcription of the partially deleted gene in shiverer mutant mice. Cell 42 (1), 149–155.
Rukov, J.L., Shomron, N., 2011. MicroRNA pharmacogenomics: post-transcriptional regulation of drug response. Trends Mol. Med. 17 (8), 412–423.
Rukov, J.L., Vinther, J., Shomron, N., 2011. Pharmacogenomics genes show varying perceptibility to microRNA regulation. Pharmacogenetics Genom. 21 (5), 251–262.
Rukov, J.L., Wilentzik, R., Jaffe, I., Vinther, J., Shomron, N., 2014. Pharmaco-miR: linking microRNAs and drug effects. Briefings Bioinf. 15 (4), 648–659.
Sangkuhl, K., Klein, T., Altman, R., 2009. Selective serotonin reuptake inhibitors (SSRI) pathway. Pharmacogenetics Genom. 19 (11), 907–909.
Schmittgen, T.D., Livak, K.J., 2008. Analyzing real-time PCR data by the comparative C_T method. Nat. Protoc. 3 (6), 1101–1108.
Schoenfeld, T.J., Gould, E., 2012. Stress, stress hormones, and adult neurogenesis. Exp. Neurol. 233 (1), 12–21.
Serafin, A., Foco, L., Zanigni, S., Blankenburg, H., Picard, A., Zanon, A., et al., 2015. Overexpression of blood microRNAs 103a, 30b, and 29a in L-dopa-treated patients with PD. Neurology 84 (7), 645–653.
Serafini, G., Pompili, M., Hansen, K.F., Obrietan, K., Dwivedi, Y., Shomron, N., et al., 2014a. The involvement of microRNAs in major depression, suicidal behavior, and related disorders: a focus on miR-185 and miR-491-3p. Cell. Mol. Neurobiol. 34 (1), 17–30.
Serafini, G., Hayley, S., Pompili, M., Dwivedi, Y., Brahmachari, G., Girardi, P., et al., 2014b. Hippocampal neurogenesis, neurotrophic factors and depression: possible therapeutic targets? CNS Neurol. Disord.: Drug Targets 13 (10), 1708–1721.
Simons, M., Nave, K.A., 2016. Oligodendrocytes: myelination and axonal support. Cold Spring Harbor Perspect. Biol. 8 (1) a020479.
Stadelmann, C., Timmler, S., Barrantes-Freer, A., Simons, M., 2019. Myelin in the central nervous system: structure, function, and pathology. Physiol. Rev. 99 (3), 1381–1431.
Steinbusch, H.W., Nieuwenhuys, R., 1981. Localization of serotonin-like immunoreactivity in the central nervous system and pituitary of the rat, with special references to the innervation of the hypothalamus. Adv. Exp. Med. Biol. 133, 7–35.
Sullivan, P.F., Neale, M.C., Kendler, K.S., 2000. Genetic epidemiology of major depression: review and meta-analysis. Aust. J. Pharm. 157 (10), 1552–1562.

TargetScanHuman 8.0 [Internet]. 2021 [cited 2022 Dec 2]. Target Scan. Available from: https://www.targetscan.org/vert_80/.
Tham, M.W., Woon, P.S., Sum, M.Y., Lee, T.S., Sim, K., 2011. White matter abnormalities in major depression: evidence from post-mortem, neuroimaging and genetic studies. J. Affect. Disord. 132 (1), 26–36.
Tkachev, D., Mimmack, M.L., Ryan, M.M., Wayland, M., Freeman, T., Jones, P.B., et al., 2003. Oligodendrocyte dysfunction in schizophrenia and bipolar disorder. Lancet 362 (9386), 798–805.
Tokar, T., Pastrello, C., Rossos, A.E.M., Abovsky, M., Hauschild, A.C., Tsay, M., et al., 2018. mirDIP 4.1—integrative database of human microRNA target predictions. Nucleic Acids Res. 46 (D1), D360–D370.
Tymofiyeva, O., Connolly, C.G., Ho, T.C., Sacchet, M.D., Henje Blom, E., LeWinn, K.Z., et al., 2017. DTI-based connectome analysis of adolescents with major depressive disorder reveals hypoconnectivity of the right caudate. J. Affect. Disord. 207, 18–25.
van Praag, H.M., Kahn, R., Asnis, G.M., Lemus, C.Z., Brown, S.L., 1987. Therapeutic indications for serotonin-potentiating compounds: a hypothesis. Biol. Psychiatr. 22 (2), 205–212.
Volk, N., Pape, J.C., Engel, M., Zannas, A.S., Cattane, N., Cattaneo, A., et al., 2016. Amygdalar MicroRNA-15a is essential for coping with chronic stress. Cell Rep. 17 (7), 1882–1891.
Williams, M.R., Sharma, P., Fung, K.L., Pearce, R.K.B., Hirsch, S.R., Maier, M., 2015. Axonal myelin increase in the callosal genu in depression but not schizophrenia. Psychol. Med. 45 (10), 2145–2155.
Woo, E., Sansing, L.H., Arnsten, A.F.T., Datta, D., 2021. Chronic stress weakens connectivity in the prefrontal cortex: architectural and molecular changes. Chronic Stress (Thousand Oaks) 5, 24705470211029256.
Wu, H.Y., Dawson, M.R.L., Reynolds, R., Hardy, R.J., 2001. Expression of QKI proteins and MAP1B identifies actively myelinating oligodendrocytes in adult rat brain. Mol. Cell. Neurosci. 17 (2), 292–302.
Wu, T., Song, H., Xie, D., Hua, K., Hu, J., Deng, Y., et al., 2020. Mir-30b-5p promotes proliferation, migration, and invasion of breast cancer cells via targeting ASPP2. BioMed Res. Int. 2020, 7907269.
xia, Huang C., Xiao, Q., Zhang, L., Gao, Y., Ma, J., Liang, X., et al., 2022. Stress-induced myelin damage in the hippocampal formation in a rat model of depression. J. Psychiatr. Res. 155, 401–409.
Yuan, Y., Zhang, Z., Bai, F., Yu, H., Shi, Y., Qian, Y., et al., 2007. White matter integrity of the whole brain is disrupted in first-episode remitted geriatric depression. Neuroreport 18 (17), 1845–1849.
Zhang, D., Liu, Z., Zheng, N., Wu, H., Zhang, Z., Xu, J., 2018. MiR-30b-5p modulates glioma cell proliferation by direct targeting MTDH. Saudi J. Biol. Sci. 25 (5), 947–952.
Zhang, Z.L., Wang, D., Chen, F.S., 2022. MicroRNA-101a-3p mimic ameliorates spinal cord ischemia/reperfusion injury. Neural Regen Res. 17 (9), 2022–2028.
Zhao, L., Ku, L., Chen, Y., Xia, M., LoPresti, P., Feng, Y., 2006. QKI binds MAP1B mRNA and enhances MAP1B expression during oligodendrocyte development. Mol. Biol. Cell 17 (10), 4179–4186.
Zhou, X., He, C., Ren, J., Dai, C., Stevens, S.R., Wang, Q., et al., 2020. Mature myelin maintenance requires Qki to coactivate PPARβ-RXRα–mediated lipid metabolism. J. Clin. Invest. Mar 23 [cited 2020 Mar 29];130(5). Available from: https://www.jci.org/articles/view/131800.
Zhu, S., Shi, R., Wang, J., Wang, J.F., Li, X.M., 2014. Unpredictable chronic mild stress not chronic restraint stress induces depressive behaviours in mice. Neuroreport 25 (14), 1151–1155.